IPP-Report

Max-Planck-Institut für Plasmaphysik

Philipp Radecker

Concept Development and Testing of an Invessel Articulated Arm for Remote Handling in ASDEX Upgrade - IVAR

IPP 2022-02
Januar 2022

Chair of Nuclear Technology
TUM School of Engineering and Design
Technical University of Munich

Concept Development and Testing of an In-vessel Articulated Arm for Remote Handling in ASDEX Upgrade - IVAR

Scientific work for obtaining the academic degree
Master of Science (M.Sc.)
at the TUM School of Engineering and Design of the Technical University of Munich

Supervisor Prof. dott. Antonino Cardella
Chair of Nuclear Technology

Advisor Dr. Albrecht Herrmann
Max Planck Institute for Plasma Physics

Submitted by Philipp Radecker
Fischerweg 14
84547 Emmerting

Submitted on December 7, 2021 in Garching

Defended on December 16, 2021 in Garching

Abstract

The present work serves to design a concept for the inspection and maintenance of ASDEX Upgrade, a fusion research experiment of the Max Planck Institute for Plasma Physics. For this purpose, a robotic arm is to be developed that can be inserted into the vacuum vessel and inspect it without breaking or contaminating the vacuum atmosphere.

After a review of known remote handling concepts, it becomes clear that none of the systems available so far meet the requirements. Therefore, in the course of a development process driven by systems engineering methods, a hyperredundant mechanism actuated via cable pulls is designed. Particular attention is being paid to vacuum compatibility and the lightweight construction of the mechanical structure.

In order to test the functionality and operation of such a remote handling system, a demonstrator is being built on a reduced scale and the corresponding software is being developed. In the first experiments, the device proves that it is sufficiently resilient and that the robotic concept can be generally verified.

Zusammenfassung

Die vorliegende Arbeit dient dem Entwurf eines Konzepts zur Inspektion und Wartung von ASDEX Upgrade, einem Experiment des Max Planck Instituts für Plasmapyhsik zur Fusionsforschung. Dazu soll ein Roboterarm entwickelt werden, der in das Vakuumgefäß eingeführt werden und dieses untersuchen kann, ohne die Vakuumatmosphäre zu brechen oder zu verunreinigen.

Nach einer Übersicht über bekannte Remote Handling Konzepte wird deutlich, dass keines der bislang verfügbaren Systeme die Anforderungen erfüllt. Daher wird im Zuge eines von Systems Engineering Methoden getriebenen Entwicklungsprozess ein über Seilzüge aktuierter, hyperredundater Mechanismus entworfen. Ein besonderer Augenmerk liegt hierbei in der Vakuumkompatibiltät sowie im Leichtbau der mechanischen Struktur.

Um die Funktionsfähigkeit und Bedienung eines solchen Remote Handling Systems zu testen, wird ein Demonstrator im verkleinerten Maßstab aufgebaut sowie die entsprechende Software dafür entwickelt. In ersten Experimenten beweißt das Gerät eine hinreichende Belastbarkeit sowie eine allgemeine Verfikation des robotischen Konzepts.

Acknowledgement

In times when home office and social distancing are the order of the day, projects that require a wide range of expertise become even more challenging. Nevertheless, it was possible for us to work together as a team within the framework of the IVAR project and to receive input from many sides. I would like to take this opportunity to thank all the people involved!

First of all, I am incredibly grateful for the academic supervision I received from Prof. Antonino Cardella. Through his great network in fusion research, he was able to put me in touch with this project. It was initiated by Irene Zammuto at the Max Planck Institute for Plasma Physics - I wish her all the best and much success on her future path at the institute. I would especially like to thank my supervisor Dr. Albrecht Herrmann, because through our regular jour fixes we solved most of the problems together. In addition, I would like to thank my colleagues from the vacuum group, Dr. Volker Rohde and Detlef Bösser, for their expertise and for carrying out the outgassing measurements.

Thanks to the excellent skills and advice of the colleagues in the Institute's workshops, we were able to turn the robot arm into reality as a demonstrator. Many thanks for that! I would especially like to thank Andreas Zeidler, Manuel Zobl and Bernhard Graf for the one or other extra hour and for 'washing my head' with regard to construction suitable for manufacturing.

Many thanks go to the Max-Planck-Gesellschaft as an institution for funding and supporting the project!

Away from the world at the Institute, there are also some people I want to thank: first my parents and my brothers for their great support in proofreading the thesis as well as going far beyond that over the last six years of my studies. I would also like to thank my friends for spell-checking and giving their opinion on my work. Special mention goes to Sharina Kimura, who was additionally responsible for the design of the logo.

Contents

List of Figures

List of Tables

Acronyms

ADC	Analog-Digital Converter
AIA	Articulated Inspection Arm
ASDEX Upgrade	Axially Symmetric Divertor Experiment Upgrade
BDSM	Bridge Transported Dual Arm Servo-Manipulator
BLDC	Brushless Direct Current
CAD	Computer Aided Design
COG	centre of gravity
CPE	Chlorinated Polyethylene
CSRM	Cable-driven Redundant Spatial Manipulator
D-H Parameter	Denavit-Hartenberg Parameter
DOF	Degree of Freedom
EAMA	EAST articulated maintenance arm
EAST	Experimental Advanced Superconducting Tokamak
EtherCAT	Ethernet for Control Automation Technology
FEM	Finite Elements Method
GCD	Global Consumption Database
GPIO	General Purpose Input/Output
I^2C	Inter-Integrated Circuit
IDE	Integrated Development Environment
IVAR	In-Vessel Articulated Robotarm
IVP	In-Vessel Penetrator
ITER	International Thermonuclear Experimental Reactor
LRR	Long Reach Robot
MFR	Multi-joint Foldable Robot
MSM	Master-Slave-Manipulator
PFC	Plasma Facing Components
PRIDE	Pyroprocess Integrated Inactive Demonstration
PVC	Polyvinyl Chloride
RGA	Residual Gas Analysis
ROS	Robot Operating System
UDP	User Datagram Protocol
UHMWPE	Ultra High Molecular Weight Polyethylene
WEST	Tungsten (chemical symbol "W") Environment in Steady-state Tokamak

Chapter 1

Introduction

1.1 Motivation and Background

The availability of energy leads to prosperity - and conversely, an augmentation of the prosperity of a society requires an increase in the supply of energy. This is clearly shown by OSWALD, OWEN AND STEINBERGER [41], based on data from the Global Consumption Database (Global Consumption Database (GCD)) and Eurostat, who find a sublinear relationship between the energy footprint and expenditure or income, which is illustrated in fig. 1.1.

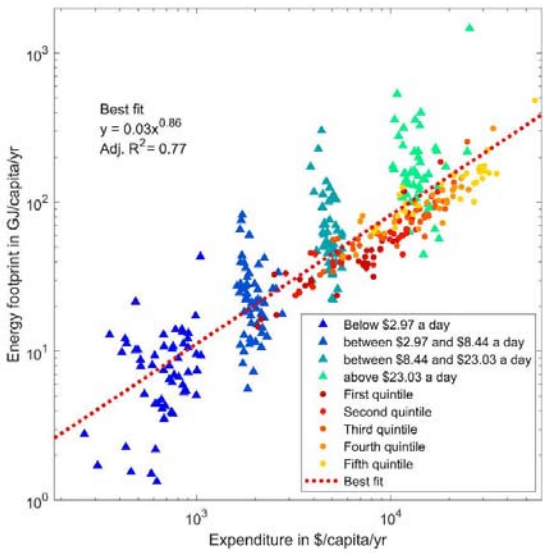

Figure 1.1: Energy footprints vs. expenditure (Triangles represent GCD data and dots Eurostat data) [41].

With an increasingly interconnected world, better living and working conditions and a further growing population, the authors justify the results of their model calculations, according to which the global energy demand will rise sharply in the coming decades.

In order to meet this demand and at the same time stop anthropological climate change, greater use must be made in the future of technologies that, unlike fossil fuels, cause no or significantly fewer greenhouse gas emissions. One of these technologies is nuclear fusion: inspired by the sun, this form of energy generation converts mass into energy through the fusion of two light nuclei into a heavier one in accordance with the theory of relativity. Currently, it is not yet possible to use them with a net energy yield, but it is assumed that the first commercial fusion power plants will be built in the second half of the 21st century, cf. fig. 1.2. MUHLICH ET AL. [39], for example, base this assumption on the fact that global strategies to avert a climate catastrophe will have to be applied in the coming years.

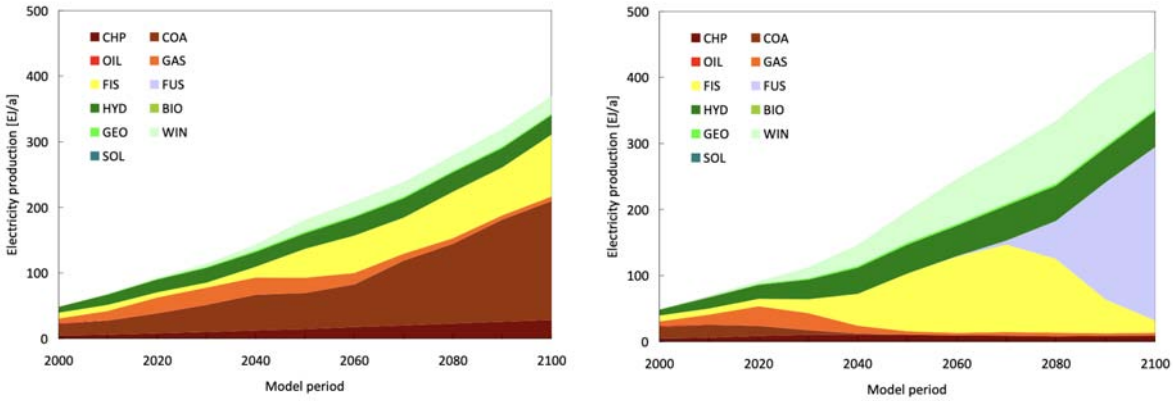

Figure 1.2: Comparison of global electricity generation mix in policy scenarios, where no greenhouse-emission limits are set (left) and where only a total atmospheric CO_2 concentration of 550 ppm is allowed (right). [39].

It becomes clear that clean energy production to meet the needs of future generations cannot be guaranteed with new renewables, like solar power plants, alone. Instead an energy mix with one or more base-load sources is needed, for which fusion reactors represent a adequate solution, as their fuel is always available and thus guarantees continuous energy production. The most promising and extensively researched design of such a reactor is the Tokamak [5]: the fusion reaction takes place in an extremely hot plasma that is confined in a circular path in an ultra-high vacuum by a very strong magnetic field. Within the vacuum vessel, exceptional thermal, mechanical and magnetic conditions prevail, which places a very high load on the materials and instruments used. A regular maintenance and inspection schedule is therefore crucial.

One of the facilities being researched to harness nuclear fusion is the Axially Symmetric Divertor Experiment Upgrade (ASDEX Upgrade) [22] whose inner vessel is shown in fig. 1.3.

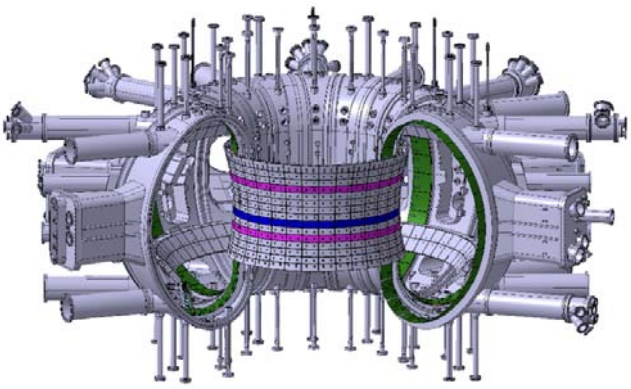

Figure 1.3: Overview of the inner vessel setup of ASDEX Upgrade [69].

Since 1991, the Max Planck Institute for Plasma Physics in Garching near Munich, Germany, has been investigating a wide range of parameters, such as the interaction between plasmas and reactor materials. Initially, the experiment was designed to remain in operation for 15 years, but due to continuous upgrades and achievements in research, successful continuation is possible even after 30 years [47]. Every year, plasma operation is suspended for a few weeks during the summer months in order to carry out conversion and inspection work on the plant. However, if maintenance work is necessary during the experimental operation

period, the unit needs to be shut down for days to weeks, as air flooding, repairing and, in particular, the subsequent evacuation and bake-out of the vessel require this time. As an example, a broken heat shield tile in the upper part of the inner first wall, highlighted in pink in fig. 1.3, led to the regular summer opening of ASDEX Upgrade having to take place two weeks earlier than planned in 2016. In this case, the use of an inspection tool could have meant that operations could have continued as planned and that around 100 plasma shots could have been carried out before the summer opening [69]. Two further examples for the which remote inspection would have been useful are given in figs. 1.4 to 1.5.

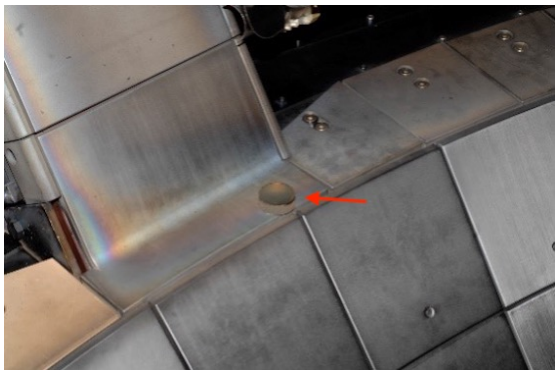

Figure 1.4: Lost glass lens due to inssuficient clamping.

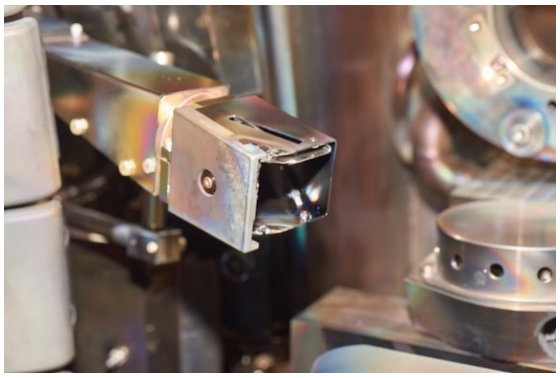

Figure 1.5: Optical front end damaged by fast ions.

Figure 1.4, taken after vessel venting, shows a glass lens that was lost during plasma operation due to insufficient clamping. The loss of *something* was detected by the video protection system. Because the *something* was not seen in later plasma discharges, it was decided not to open the vacuum vessel for inspection.

An optical front end is depicted in fig. 1.5. During operation, a loss of intensity was detected. A reason could not be identified. In-vessel inspection after venting reveals, that fast ions coming from the neutral beam injection hit the front end which results in a melting of the protection cap and a damage of the lens.

1.2 Objectives

The original design of ASDEX Upgrade did not include the possibility of using a remote handling system to carry out investigations and maintenance work in vacuum between plasma shots. Developing one can prevent the vessel from opening in the event of future unforeseen events, saving valuable time for the experiments. In addition, a set of unexpected events are monitored during plasma experiments, such as hot spots due to high energy impact or loss of intensity in light detecting diagnostics. Identifying the reasons and in particular the consequences for future operation requires experimental time. In vessel inspection would allow a direct survey and a reliable risk estimation.

For this reason, the aim of this thesis is to design a robot arm that can be introduced into ASDEX Upgrade without having to fundamentally modify the vessel and while maintaining the vacuum atmosphere. This robot should be able to map a torus with its working space in order to inspect the entire vessel from the inside. In addition, the payload should be sufficient to carry tools such as grippers, lights and cameras and, if necessary, to pick up contaminants and remove them to the outside. Due to its tokamak-specific design, the robot could serve as a template for future fusion experiments and commercial reactors. In addition, such a

machine can also be used for other tasks in fusion technology, such as the precise calibration of measuring systems.

Validation of the concept is a second objective: a demonstrator is to be set up to prove the function of the individual components in interaction and to develop a suitable control and interaction approach. Attention should be paid to modularisation and, if possible, to reusability for the final robot.

The project was given the name In-Vessel Articulated Robotarm (IVAR)[1] and a corresponding missionpatch has been created as depicted in fig. 1.6.

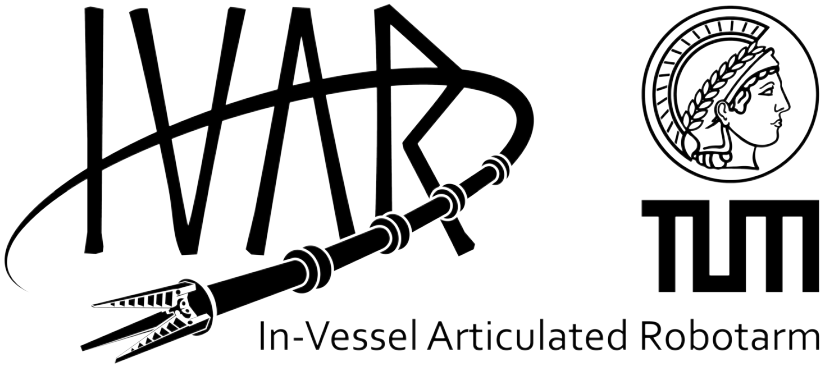

Figure 1.6: Missionpatch of the IVAR project.

1.3 Organization of the Thesis

To introduce the topic, chapter 2 first gives an overview of the current state of the art in research and industry. It will be shown to what extent the topic of remote handling for fusion experiments has already been addressed. Preliminary work that deals with the development of mechanisms for vacuum applications and those that explain the concept of hyperredundant robots will also be discussed.

Based on these, a concept for the implementation of an inspection and maintenance robot for ASDEX Upgrade is built in chapter 3. Following systems engineering methods, alternatives will be weighed up based on the requirements and finally a proposal for an optimal model will be made.

Chapter 4 describes the construction of a demonstrator, which is to serve as a proof of concept. Both the developed hardware and software components for the successful operation of the demonstrator will be presented.

Subsequently, the results are discussed in chapter 5 and further existing problems are pointed out.

Finally, chapter 6 summarises the work and gives an outlook on further research approaches.

[1]The project was not only given the acronym IVAR from its function. Furthermore, this name was chosen because there is a matching figure in Norse mythology that bore this name [59]: Ivarr the Boneless, one of Ragnar's sons and a leading participant in the Viking conquest of eastern England, was, according to stories, born with glass bones and thus had to move like a snake throughout his life which corresponds to the movements of the articulated arm.

Chapter 2

State of the Art

The state of science and technology is roughly divided into three parts. First, an overview of remote handling concepts will be given, as they are used in other applications. In particular, it will be shown how robotic systems are used in fusion research to date. The second part shall be dedicated to the requirements that the environmental conditions place on the inspection task. Special attention is paid to the vacuum application and the materials that shall be used. Finally, hyperredundant, tendon-driven robots are to be addressed. The special features with regard to their construction, actuation and control will be highlighted and it will be made clear that, despite the high complexity, their advantages for the intended application outweigh those of other concepts.

2.1 Remote Handling Concepts

Remote handling is necessary wherever environmental conditions make it impossible for humans to carry out the work. Well-known examples include robots for bomb disposal [38] or maintenance arms on spacecraft [58]. Basically, a remote handling system always describes the possibility of handling objects and tools teleoperatively. This does not necessarily have to be carried out by a robot or another mechatronic system as simple waste grippers also can be classified as remote handling systems.

2.1.1 Development of remote handling systems

BECQUET [6] therefore identifies eight aspects that are of particular importance in the design of robotic remote handling systems and which will be described in the following. The mechanical design must first meet the requirements of the geometric constraints as well as the payload. In addition, special specifications may arise due to environmental influences such as radiation or even the use in high vacuum. The next step is to find a suitable principle for actuation: hydraulic actuators allow high loads to be moved with limited precision, whereas piezoelectric actuators, for example, allow positioning on a scale of nanometres, but cannot apply large forces. Then the control of the system must be considered, which also increases in complexity with an increasing number of Degrees of Freedom (DOFs). Often, a classical approach is not possible here due to many singularities and so modern methods such as neural networks or genetic algorithms are increasingly used today. The use of closed control loops also requires the selection of suitable sensors, which differ both in their physical measurement principles and in their precision. Steps five and six relate to the human-machine interface: on the one hand, suitable inspection tools, such as cameras and probe heads, must

be implemented and the recorded data must be made available to the operator and visualised in realtime. On the other hand, an interaction between operator and robot must be possible that allows all functionalities of the system to be used and enables operation that is as intuitive as possible. Finally, BECQUET lists two points that concern the general design: solutions should always be implemented that are easily accessible and leave room for extensions, because especially in the industrial environment this offers optimisation potential through future upgrades. And, most importantly, he names the reliability of the system which, if possible, should be tested with all available tools, such as simulations and the application of reliability engineering methods.

2.1.2 Industrially used remote handling systems

Robotic remote handling applications have their origins in nuclear technology, because the handling of fissile material has always required special caution [30]. These first so-called master-slave manipulators translate human movements linearly to a mechanical system, which in turn is in direct contact with the hazardous environment. As an example, fig. 2.1 shows the concept of a master-slave manipulator as used for the Pyroprocess Integrated Inactive Demonstration (PRIDE) facility in Korea [31].

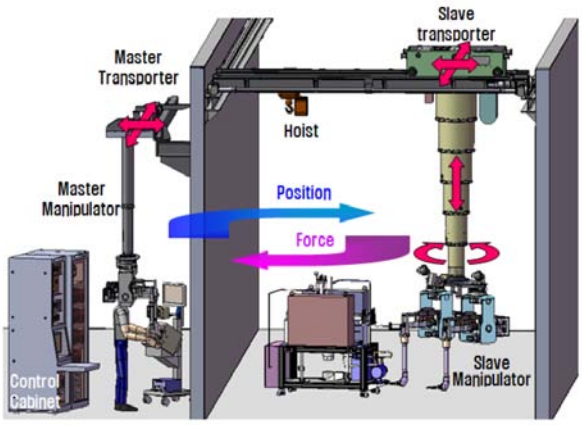

Figure 2.1: Concept of the remote operation and maintenance system in argon cell of the PRIDE facility [31].

The PRIDE facility is designed to test several main process equipments such as a vol-oxidizer, an electrolytic reduction, an electro refining, an electro winning, etc., where these are installed at an argon atmosphere cell. The remote handling system for the PRIDE facility consists of remotely operated devices such as a Bridge Transported Dual Arm Servo-Manipulator (BDSM), wall mounted mechanical Master-Slave-Manipulators (MSMs), and a crane. Among these equipments, the BDSM system has been developed to realize a successful operation and maintenance of a Pyroprocess. The system has dual arm servo-manipulator where each arm has 6 DOF with a payload of 25 kg, a 4-DOF bridge transporter, and a control station with visual display panels.

Another example of robotic systems used in nuclear technology is the Snake Arm Robot from the British company OC Robotics [40]. As BUCKINGHAM AND GRAHAM [9] describe, they were used, among other projects, for repairs to the steam pipes of the Swedish Ringhals I. nuclear power plant. These hyper-redundant, multi-jointed, cable driven manipulators were able to inspect the pipe, cut it using a laser cutter and rejoin it by orbital welding. fig. 2.2 shows the application of the robots in Ringhals and Pickering (Ontario, Canada). Although the robots use the same basic principles, they look very different. This is primarily because such systems are always designed for a specific purpose in order to meet all the demands

Figure 2.2: Snake arm robots in the nuclear powerplants Ringhals, Sweden (left), and SAFIRE robot in Pickering, Canada (right) [9].

placed on them: as can be seen on fig. 2.2, the Ringhals robot shown on the left is introduced linearly and can move omnidirectionally, whereas the robot shown on the right, which was used in Pickering, can be unwound from a kind of barrel and can only operate degrees of freedom in the horizontal plane.

2.1.3 Remote handling for fusion engineering

For the special purpose of inspecting a fusion reactor's vacuum vessel, there are also already some studies which will be used in the following. The greatest progress was made on the research experiments Tungsten (chemical symbol "W") Environment in Steady-state Tokamak (WEST) [7], formerly Tore Supra [8], and the Experimental Advanced Superconducting Tokamak (EAST) [62], and some concepts were presented for the International Thermonuclear Experimental Reactor (ITER) [23], which is currently under construction.

For EAST, SHI ET AL. [50] designed a 10-DOF inspection arm, the EAST articulated maintenance arm (EAMA). The concept is described schematically in fig. 2.3.

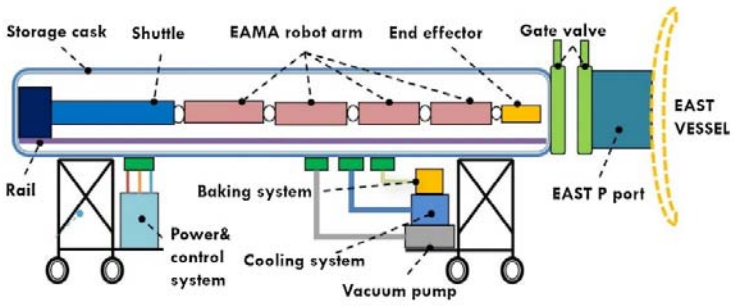

Figure 2.3: Overall schematic view of the EAMA system [50].

The robot is capable of operating at an atmospheric pressure of 10^{-7}mbar and an ambient temperature of 80 °C. With a net mass of about 100 kg, it is possible to move 25 kg payload, which is a very high payload to mass ratio compared to other industrial robots. This is made possible by a paralellogram structure inside the individual links, which serves as gravitational compensation. The actuation takes place via linear actuators inside the tubes, which in turn

control the rotational joints via cables and pulleys. The individual components are shown in fig. 2.4.

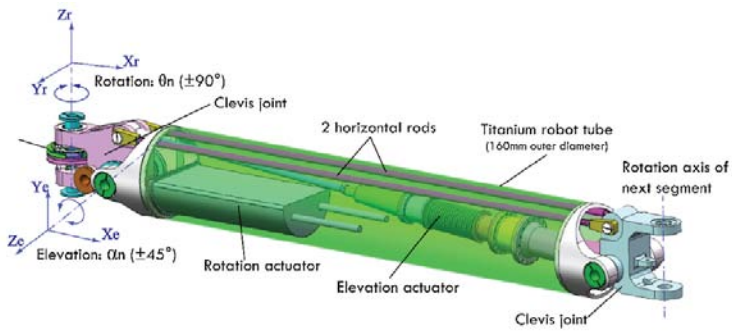

Figure 2.4: Components of an EAMA segment [50].

Unlike ASDEX Upgrade, EAST was designed to be able to connect such a robotic inspection tool externally. Therefore, fig. 2.3 shows a gate valve that is connected to the storage cask of the robot. This made it possible to realise the design of the arm with a diameter of 160 mm. PAN ET AL. summarise the findings obtained from the experiments with the EAMA [42]. Among other things, a general proof of concept of a maintenance arm was achieved in a fusion experiment, but individual components, such as the vacuum-compatible lubrication and the sensor technology, were also validated.

A similar approach is taken by PERROT ET AL. with the Articulated Inspection Arm (AIA) [44]. Building on the knowledge previously gained with the In-Vessel Penetrator (IVP) [45], a remote handling system was developed that is to be used for the maintenance of ITER. While the geometrical boundary conditions are similar to those of ASDEX Upgrade a particularly high demand is placed on the temperature resistance, since an ultra-high vacuum must also be maintained between the plasma shots. This requires the components of AIA to be baked out, which is why the main focus of the investigations was on temperature durability. The actuation principles are similar to EAMA, i.e. each joint is controlled by linear actuators located in the links. This decentralised actuation increases the mass and thus the lever load of the whole structure. This has a negative impact on the robot's precision and necessitates extremely expensive military-grade components. Nevertheless, AIA was successfully realised and tested in WEST and the Tore Supra mock-up respectively, see fig. 2.5.

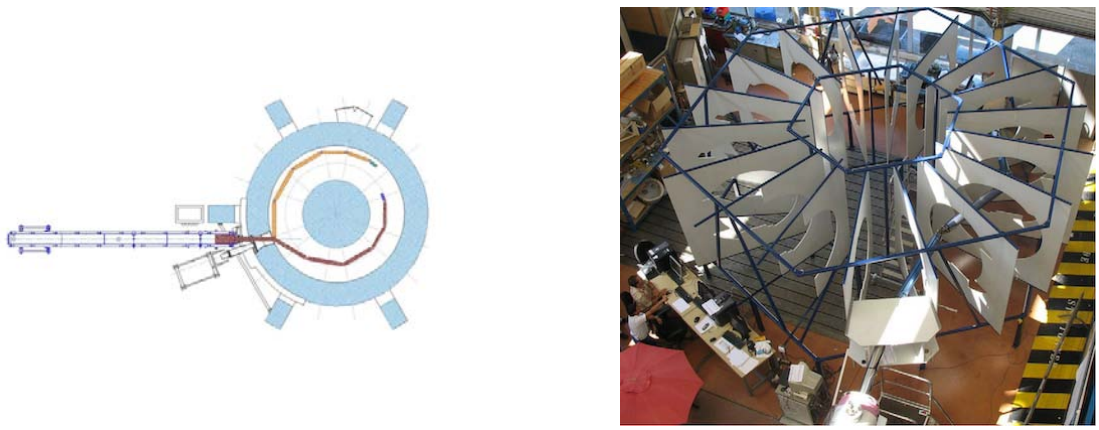

Figure 2.5: Visualisation of accessibility within WEST (left) and AIA prototype introduced in the Tore Supra mock-up (right) [55].

As can be seen in the illustrations, AIA also represents an extremely long and slender

structure that can be inserted through a diagnostic port measuring 250 mm. In numbers, the length of the actuated arm is 8 m and comprises five modules, each 160 mm in diameter. These are made of titanium to withstand the high lifting loads and at the same time be as light as possible. In addition, as with EAMA, a parallelogram structure is used to balance gravity. A viewing system able to make accurate visual inspection of Plasma Facing Components (PFC) under darkness conditions is installed at the front head of the carrier [19]. After the proof of concept, various diagnostic tools were developed for AIA. Among other things, a sniffer system for leak localisation and a gamma camera for the examination of radioactively contaminated components were realised [25].

As a final example of inspection systems for fusion experiments, the work of WANG ET AL. at the Chinese Academy of Sciences should be cited. First, a so-called Long Reach Robot (LRR) was designed [64]. In contrast to the concepts presented so far, the actuation of the LRR is decentralised, i.e. the drives are located at the end of the cantilever structure and the actual joints of the arm are moved from there via the relative movement of cables. In terms of structural design, this has the advantage that the mass of the arm is considerably less than with AIA or EAMA. This makes aluminium a much cheaper alternative to titanium as a material for the segments, despite its lower strength. The LRR is depicted in fig. 2.6.

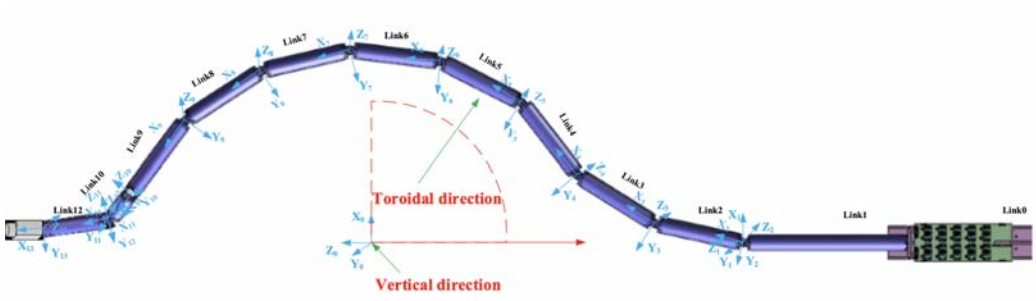

Figure 2.6: Schematic representation of the LRR. The local coordinate systems of the individual links are shown [63].

The illustration makes it clear that the heavy part of the robot, namely the linear slide shown in green with the motors and pulleys, remain outside the arm structure. Adjacent to this is a fixed feed tube of 1.2 m in length. This is followed by eight horizontally movable links, each 660 mm long, and one 220 mm long link. The instruments are attached to the last link, which is also 660 mm, and it can operate an additional degree of freedom in the vertical plane. Overall, the robot is hyperredundant with 12 DOF, 8 m reach and the arm structure weighs 35 kg, only about a quarter of that of AIA or EAMA. This makes it possible to precisely move a payload of about 5 kg.

In 2017, the same research group presented a second remote handling project based on this: the Multi-joint Foldable Robot (MFR). WU ET AL. [34, 61] developed this articulated arm as a flexible, mobile inspection tool to maintain EAST. As with EAMA, they make use of the gate valve, which is why the concept cannot be used for other experiments without a maintenance opening for geometric reasons. Here, too, a cable-driven system is used, but the engineers decided to house the motors in the individual parts of the arm. This in turn increases the structural load and brings problems with the deflection and precision of the robot. To date, the MFR is the latest approach to a vacuum vessel inspection system for fusion devices.

2.2 Robotics in Vacuum Environments

When thinking of robots in a vacuum, the first thing that comes to mind is generally systems in space missions as described by WANG ET AL. [58]. While certain requirements are similar, such as the absence of convective heat transport, it is above all the requirement not to pollute a vacuum vessel that makes the application very different. According to ISO 3529 [27], the degree of vacuum application can be divided into four classes: Low, Fine, High and Ultra High Vacuum. Parts used in the respective class must therefore be examined for their material properties. WUTZ ET AL. [65] make two types of demands on materials used in vacuum technology:

1. those that are specifically of a vacuum-technical nature:
   (a) gas tightness
   (b) low inherent vapour pressure (saturation vapour pressure; melting and boiling temperature must be observed)
   (c) low foreign gas content (easy degassing)
   (d) clean surfaces (no or easily removable adsorbed layers)
2. and those that are caused by the vacuum processes:
   (a) chemical resistance to gases and vapours
   (b) thermal expansion behaviour
   (c) thermal shock resistance
   (d) mechanical strength

Experimental data and tables must therefore be used to select suitable materials. For example, if the application takes place at a temperature of 300 °C and in a ultra high vacuum ($\leq 10^{-6}$mbar), magnesium components cannot be used because their vapour pressure is higher at this point and the material thus evaporates, see fig. 2.7.

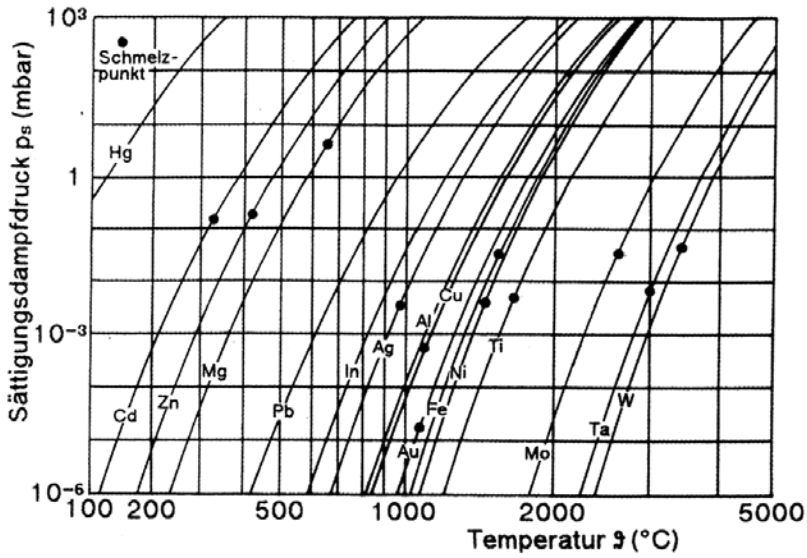

Figure 2.7: Vapor pressure curves of various substances [65].

The same applies to tin-based solders or lubricants, for which vacuum-compatible alternatives must be selected. Guidance can be found in the work of WUTZ ET AL. [65].

Especially when designing the drives, the vacuum requirement is crucial. Usually, care is taken to position the actual motor components outside the vacuum chamber and to insert the output shaft by means of vacuum rotary feedthroughs [65]. If this is not possible due to the design of the device, because the drive unit must move along with the robot, for example, vacuum-compatible motors must be found. Here, too, a distinction is made between whether the drives are used only once, possibly with a precalculated, severely limited service life, or whether continuous operation takes place. The former is often the case in space applications where, for example, the solar sails have to be unfolded once after the launch of a satellite and thus it can be accepted that the drive is already worn out after a single use. This means that well-sealed standard components can also be used, which benefits both the design and the financial effort. In the case of a continuously operating mechanism, YATES [67] suggests several concepts for motion design. In addition to actuators based on shape memory alloy, he discusses, among other things, possibilities to design modern servo motors in such a way that the materials used do not outgas within the specified limits, the lubricants of the bearings do not become ineffective and the drives do not fail despite the lack of possibility to dissipate heat via convection. Manufacturers of modern high-performance servo motors, such as Maxon[37] or Faulhaber [17], make use of these principles in the drive design and offer servo motors with a specification for the different vacuum classes.

2.3 Hyperredundant Robots

The hard requirements for the design of the robot listed in chapter 3 quickly rule out concepts such as mobile, fixed or humanoid robots for the inspection of the vacuum vessel. Therefore, the following part is dedicated to the ideas of the so-called hyperredundant robots, as they have already been applied in other fusion experiments.

2.3.1 Design

Basically, hyperredundant or continuum robots are inspired by biological structures. KOLACHALAMA AND LAKSHMANAN [29] created an overview of the biologically inspired mechanisms: in particular, the movement abilities of the snake, the octopus tentacle and the human spine are often adapted for robotic applications. What they have in common is that the ratio of their length to their diameter is comparatively large and, by actuating many internal degrees of freedom, they are able to curve around objects and thus move elegantly in complex environments. This redundancy of degrees of freedom gives them their name.

Research into this is being carried out at many institutes around the world: a research group at the Tokyo Institute of Technology, for example, has developed the Super Dragon [14]. This 10 m long manipulator, in its final design, is intended to decommission harboured nuclear power plants, such as the one in Fukushima. Due to the high radiation exposure and the impassable access, a remote handling system is indispensable. The operating principle and the design of the Super Dragon are presented in fig. 2.8 respectively fig. 2.9.

With 21 actuators, the Super Dragon can operate 10 degrees of freedom to inspect complicated geometries. In addition, there is a payload of 10 kg, which enables the attachment of laser or waterjet cutting devices. The details of the actuation are described in more detail in section 2.3.2.

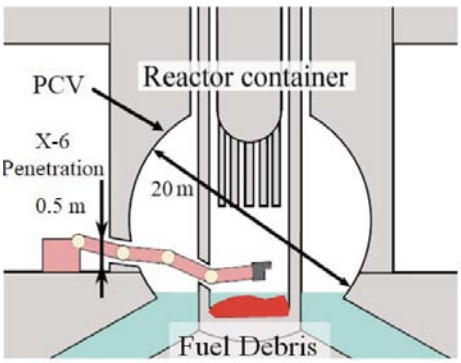

Figure 2.8: Operating image of deployment in the Fukushima Power Plant [14].

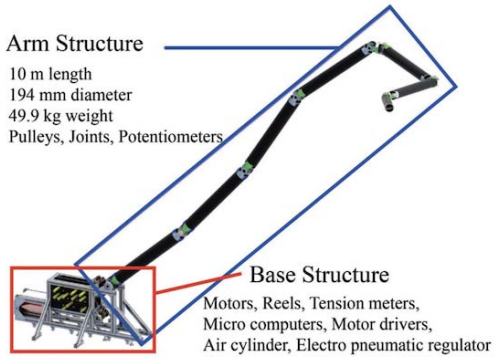

Figure 2.9: 3D-CAD model of the Super Dragon [14].

While the Super Dragon was designed specifically for use in Fukushima, the Harbin Institute of Technology in Shenzhen, China, is researching the more versatile, Cable-driven Redundant Spatial Manipulator (CSRM) [32], which can serve various purposes thanks to its modularity. Among other things, it will serve as a template for future maintenance arms on spacecraft and be used for the inspection of pipelines by mobile robots. LIU ET AL. begin their work by comparing four basic structures for building a cable-driven, hyperredundant robot and compare them in terms of their main parameters. These structures are shown in fig. 2.10.

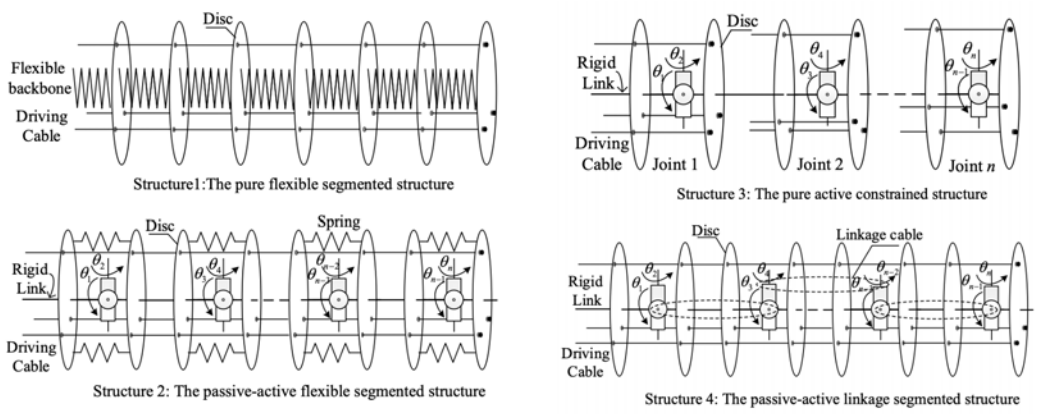

Figure 2.10: Characteristic structures for mulitlink hyperredundant robots [32].

While 'Structure 1' has a flexible backbone and works without rigid parts, 'Structure 2' relies on rigid links that are flexibly connected to each other in the area of the joints. 'Structure 1' therefore has an almost continuous form and 'Structure 2' an actively-passively coupled, discrete form. On the one hand, 'Structure 3' offers the most possibilities due to the individual control of all links, but it also requires the most drives and offers the highest complexity. 'Structure 4', the one preferred by the authors, also relies on a connection between the links in order to realise a uniform and less complex movement. Unlike 'Structure 2', however, Bowden cables are used here instead of elastic elements, which allows a higher force transmission and a more precise determination of the relative angles. The performance of the structures is compared in the table in table 2.1.

As can be seen in the table, 'Structure 4' outperforms the others in terms of almost all comparative values. Only 'Structure 3' has a higher load capacity, but this goes hand in hand with a maximisation of the number of drives and thus with the highest complexity and the

Structure	1	2	3	4
Load capacity	low	low	the largest	large
Mass	big	big	less	less
Torsional rigidity	small	high	high	high
Motors number	less	less	maximum	less
Kinematics model	complex	complex	simple	simple

Table 2.1: Comparison of different structures [32].

worst cost-effectiveness. The authors decided to use a robot according to 'Structure 4' as shown in fig. 2.11 and fig. 2.12.

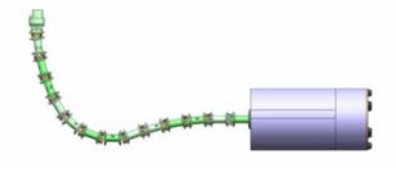

Figure 2.11: Design of the CSRM [32].

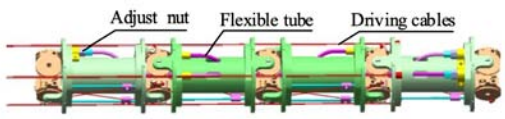

Figure 2.12: One distinct segment of the CSRM [32].

The finished CSRM consists of three segments with four links each, which were linked to each other with Bowden cables. In experiments, the CSRM achieved a payload capacity of 1.5 kg and a high precision in pick and place tasks.

Examples of robots according to structural principles 1 to 3 are provided by YESHMUKHAMETOV ET AL. [68], WANG ET AL. [57] and WU ET AL. [60].

2.3.2 Actuation

Basically, two principles can be used to actuate the joints: either they are driven directly on their motion axes or via decentralised force guidance. PAN ET AL. [42] use the former by building the linear actuators directly into the links in EAMA. The advantage of this design is the direct power transmission and the simpler control. The disadvantage is that with an inspection arm the mass and thus the load on the bearing point and the links increases considerably.

Therefore, the decentralised path is preferred in many approaches. Both Liu et al. [32] and TANG ET AL. [51] use a power transmission via cables. In both concepts, the wire ropes are tensioned via linear spindle drives and thus deflect the individual joints. ENDO ET AL. [14], on the other hand, wind the ropes onto pulleys, which saves space but also requires more powerful motors. In addition, instead of stainless steel wire ropes, they use plastic ropes made of Ultra High Molecular Weight Polyethylene (UHMWPE) fibres, which have a significantly higher breaking load with reduced density [4].

Finally, with regard to vacuum compatibility, there is the question of the actual drives. For EAMA [42] as well as for other already realised concepts for fusion experiments, only special servo motors can be considered that both fulfil the performance requirements and do not pollute their environment through appropriate sealing, the use of appropiate materials and prior degassing.

2.3.3 Kinematics and control

When developing hyperredundant robots, a comprehensive kinematic analysis is crucial. The fact that the same degrees of freedom are manipulated by several joints creates sigularities that make classical forward and backward kinematics according to CRAIG [11] impossible. However, the Denavit-Hartenberg parameters he describes can still be used by working with pseudoinverses. KIRÉANSKI AND PETROVIÉ [28] used this method, known mainly from structural mechanics, to determine the backward kinematics of their 7-DOF robot. For general 2n-DOF spherical joints, LOU ET AL. [35] developed a closed-form solution for inverse kinematics. However, they assume that the applied forces are distributed at regular angular intervals on the joint plates. XU ET AL. [66] simulate the kinematics for both a 12-DOF and a 20-DOF hyperredundant robot by combining multiple links into uniform modes and using a spline-based algorithm. Their approach is also only applicable to joints of the same type.

With regard to the control logic, two possibilities are pursued to form a closed control loop. Either the actuator positions are directly measured via encoders and calibrated with reference switches [33] or there are angle sensors directly at the joints that report the absolute position [14] [60]. What they all have in common is that they use a nose-following principle when introduced into the environment under investigation, where the movement of the first link is copied by the following ones. TANG ET AL. [52] describe four algorithms that can be used to plan the movement of the individual joints: optimisation search, bisection search, iterative search and prediction lookup.

Chapter 3

Concept Development

After a detailed analysis of the state of the art in chapter 2, it is noticeable that the already realised inspection concepts of other fusion experiments are similar in nature, but were always developed together with the devices to be maintained. What is missing is an universally applicable tool that is versatile enough to be used for applications that have not been specially adapted for this purpose. One such application is the inspection of ASDEX Upgrade between plasma shots. Up to now, it has only been possible to inspect parts of the torus.

For this reason, the following chapter is dedicated to the purpose of developing a remote handling concept with the help of systems engineering methods. To this end, the requirements for such a device are first defined. In the following sections, different options regarding design, actuation and control are discussed and the preferred approach is presented.

3.1 Systems Engineering

The principles of systems engineering, which are mainly known from the aerospace industry, can also be applied to projects such as IVAR. HABERFELLNER ET AL. [21] provide developers with helpful tools to reduce the effort of project management to a minimum and at the same time ensure constant quality control. The system development process is shown in fig. 3.1.

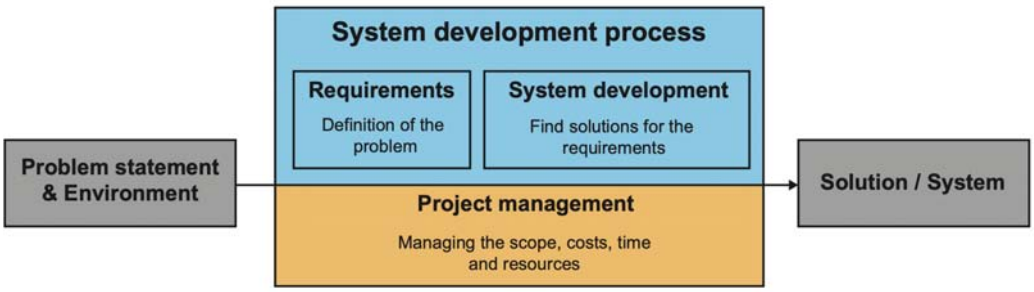

Figure 3.1: System development process (based on the lecture notes by WALTER [56]).

The problem statement has already been formulated. The environment adopted is primarily ASDEX Upgrade, but ideally the system should be developed in such a way that it can also be adapted for future projects with minor adjustments. The entire product development process should be accompanied by functioning project management, which is achieved through advance planning, weekly jour fixes and constant documentation of the results. The process itself is based on the general Vee model as shown in fig. 3.2.

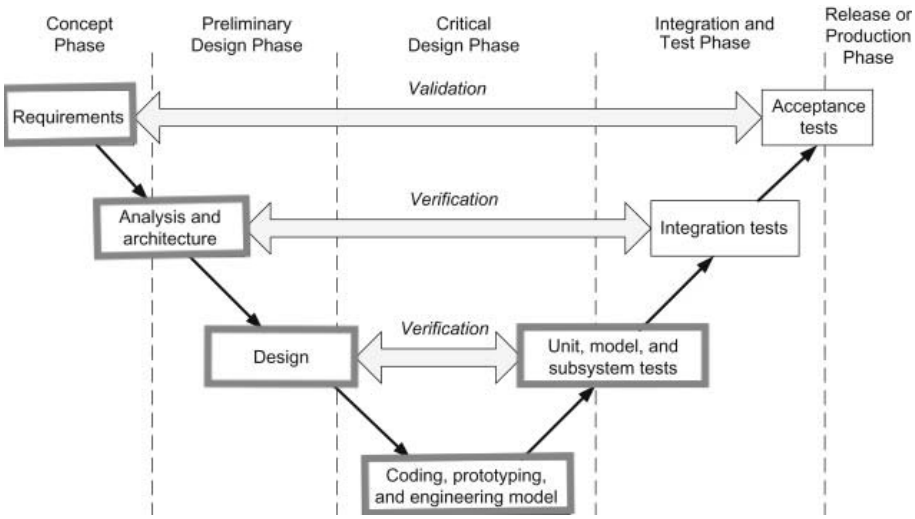

Figure 3.2: General Vee model [18].

Due to the limited time of the master thesis and the personnel capacities, only one iteration of the ascending arm can be executed for verification. This will be done as described in chapter 4 by setting up a demonstrator, with the help of which the first important components will be tested. The development therefore goes through the Concept Phase, the Preliminary Design Phase, the Critical Design Phase and the first stage of the Integration and Test Phase.

3.2 Requirements

At the beginning of a system development process, the requirements are formulated and documented in a specification sheet. The requirements arise according to HABERFELLNER ET AL. [21] from the wishes of the customer, the feedback of the developers and ultimately from the constraints that the environment imposes on the system. In this case, the customer is the Max Planck Institute for Plasma Physics. The problem statement and the general functional requirements therefore result from agreements with the project initiators. This includes:

- "REQ-01: The inspection of the vacuum vessel of ASDEX Upgrade must be possible between plasma shot days"
- "REQ-03: The device must be able to be inserted through the port of the midplane manipulator"
- "REQ-04: The workspace must be able to map the torus of ASDEX Upgrade"
- "REQ-05: The vacuum must not be contaminated"
- "REQ-06: The unit must have a payload of at least 2 kg"
- "REQ-07: Instruments for inspection (camera, light, gripper) must be able to be attached"
- "REQ-12: The system should be able to be stored in the Torus hall when not in use"

Together with the vacuum operations group at the institute, this also defined the boundary conditions for operation under very low atmospheric pressure. Normally, ASDEX Upgrade operates in an ultra-high vacuum atmosphere of less than 10^{-6}mbar, but the pressure can be

increased to 10^{-3}mbar without requiring a subsequent bake-out. This benefits the selection of suitable components and is incorporated into the following environmental conditions:

- "REQ-02: Operation must be possible at an atmospheric pressure of less than 10^{-3}mbar"
- "REQ-04: The workspace must be able to map the torus of ASDEX Upgrade"

Finally, in the course of the development, requirements were also defined that serve the adequate operation of the remote handling system:

- "REQ-08: The device should be modular in terms of usable instruments and future upgrades"
- "REQ-09: The travel speed should be greater than or equal to 0.25 m min^{-1}"
- "REQ-10: The position and orientation of the unit should be verifiable at all times"
- "REQ-11: The system should be intuitive to use"

The quality function deployment diagram in fig. 3.3 was created to document the requirements.

Category 1 = must have ● = strong relationship
Category 2 = should have ■ = moderate relationship
Category 3 = nice to have ▲ = possible relationship
X = correlation

ID	Category	Requirements / Characteristics / Subsystems	Vacuum compability	Articulated mass	Control	Actuation	Connection	Instruments
REQ-01	1	The inspection of the vacuum vessel of ASDEX Upgrade must be possible between plasma shots	●	●		▲	●	■
REQ-02	1	Operation must be possible at an atmospheric pressure of less than 1e-3 mbar	●			■	●	▲
REQ-03	1	The device must be able to be inserted through the port of the midplane manipulator			■	●	●	▲
REQ-04	1	The workspace must be able to map the torus of ASDEX Upgrade			●	■		
REQ-05	1	The vacuum must not be contaminated	●					■
REQ-06	1	The unit must have a payload of at least 2 kg		●	■	●		●
REQ-07	1	Instruments for inspection (camera, light, gripper) must be able to be attached						●
REQ-08	2	The device should be modular in terms of usable instruments and future upgrades	▲	▲				●
REQ-09	2	The travel speed should be greater than or equal to 0.25 m/min			■	●		
REQ-10	2	The position and orientation of the unit should be verifiable at all times		▲	●			
REQ-11	3	The system should be intuitive to use			●	●		
REQ-12	3	The system should be able to be stored in the Torus hall when not in use					■	

Figure 3.3: Quality function deployment diagram.

This diagram serves as a guideline for the entire development process and, after a detailed evaluation of the requirements, shows relationships to the characteristics or to the

subsystems. It also makes it possible to create a correlation matrix between the characteristics of the system and thus make the consequences of design changes assessable. In its structure, it is based on that of AKAO's method of the House of Quality [1].

3.3 General Design

Once the requirements have been formulated, the preliminary design phase can begin. Fixed remote handling systems are ruled out, as they require extensive changes to the design of ASDEX Upgrade. Thus, the choice falls on a mobile robot that can be connected to the midplane manipulator port, enclosed in a vacuum container. This port consists of an opening with a diameter of 89 mm, which can be closed by a gate valve. A linear slide with a supported vacuum bellows is attached to the outside, allowing a travel distance of 1900 mm. The setup is depicted in fig. 3.4.

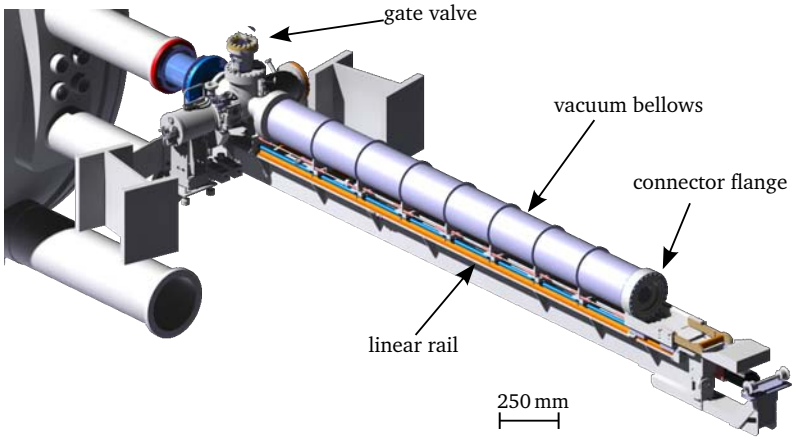

Figure 3.4: 3D-CAD representation of the midplane manipulator port.

It can be seen from the figure that only an ultra-slender structure can be introduced. This has a direct impact on the options available for the general design of a remote handling robot: as with previously known approaches, an articulated arm structure should also serve for this purpose.

Due to the geometry of the vacuum vessel with a major radius of 1.65 m, REQ-04 requires an arm length of at least 5 m to be able to map a half torus with one horizontal movement clockwise and one counterclockwise. In addition, a vertical movement of at least 1 m upwards and downwards must be possible to completely examine the vessel with a height of 2 m. Therefore, an arm with 6 m articulated length shall be designed. In addition, there must be a rigid feed link to cover the distance from the connector flange, via the gate valve, to the entry into the inner wall of the vessel.

The ratio of the articulated length to the diameter of the unit is structurally challenging. Care must be taken to reduce the mass of the cantilevered part of the system as much as possible. Furthermore, appropriate materials need to be selected to make the structure both light and resistant to the load cases that occur. In addition, the design is to be checked structurally using the Finite Elements Method (FEM).

In order to estimate the number of DOFs required, the planned sequence of the inspection process must be considered. The idea is similar to WU ET AL. [63] and is divided into five steps:

1. First, the robot is in the vacuum enclosure until the insertion process starts.
2. Then it is introduced linearly and performs the first curve to avoid hitting the inner wall.
3. This is immediately followed by a movement in the opposite direction of rotation in order to remain on the circular path.
4. This movement continues until the target is reached.
5. There, the tip of the arm orients itself both horizontally and vertically to carry out inspection work.

The key frames of the inspection process are described in fig. 3.5.

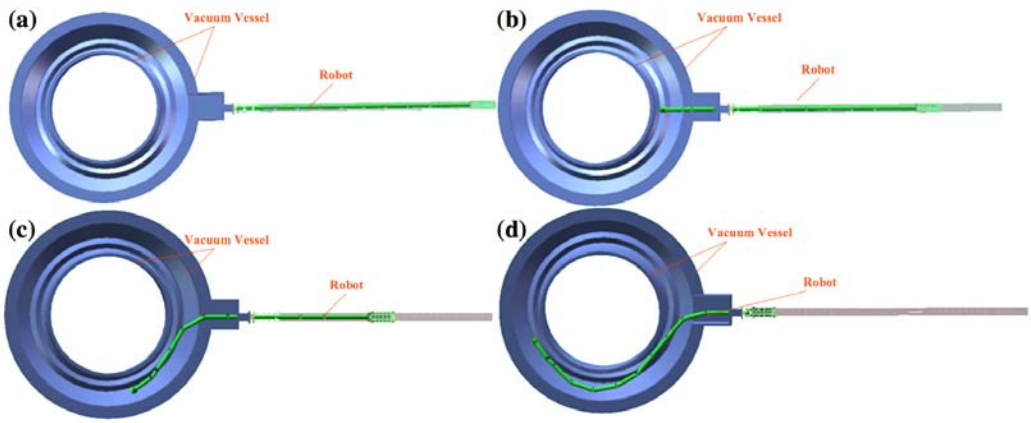

Figure 3.5: Key frames of inspection procedure: **a** in the storage cask, **b** move in/out the vacuum vessel, **c** arrive at the midway location, **d** arrive at the destination [63].

The process results in one translation and four rotations as the minimum number of DOF. The former can be achieved by mounting the arm on a linear axis located in the vacuum enclosure. However, only three rotational DOF in the horizontal plane would mean that the 6 m long arm would have to be divided into three links, each 2 m long. This design is not possible because the distance between the entrance port and the inner wall is only 1.4 m. It therefore makes more sense to allow at least five rotations in the horizontal plane and to limit the length of each segment to 1.2 m. With regard to movement in the vertical plane, this length is also sufficient, but a single rotation around this axis means that every position of the vessel wall can be reached, but not in every pose. Therefore, redundancy should also be achieved here by providing the foremost two segments with an additional DOF in the vertical plane, see fig. 3.6

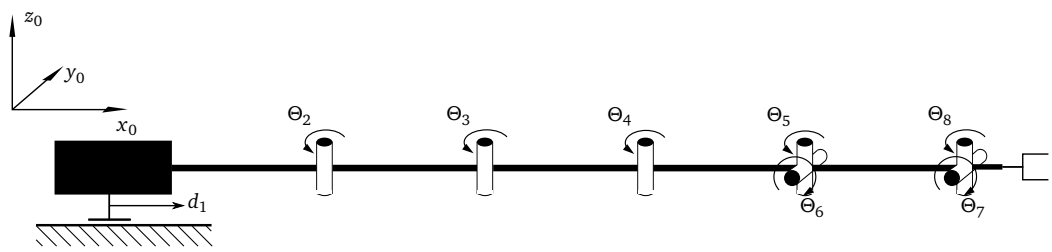

Figure 3.6: Sketch of the concept with the necessary DOF.

So the basic structure of the remote handling system is set: an articulated arm with seven DOF is to be developed, which is mounted on a linearly movable carriage.

3.4 Actuation

Once the general design has been determined, the concept must be refined in terms of its actuation. As already taken up in chapter 2, an articulated robotic arm can be based on two principles: either motors drive the joints directly on their axes or they are centrally mounted in a motor box and their movements must be transmitted to the joints. The former offers the advantage of efficient and direct power transmission. However, the principle cannot be applied because the weight of the drives makes the leverage forces so great that no commercially available motor-gearbox combinations with suitable dimensions can provide sufficient power.

Therefore, a motor box is designed from which cables are drawn to the respective joints to move them. This is shown in fig. 3.7.

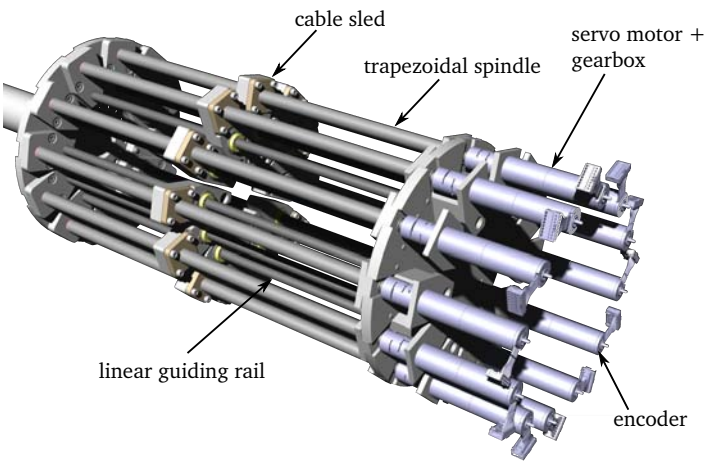

Figure 3.7: Actuation unit.

The actuation unit consists of motor-gear-encoder combinations, each of which drives trapezoidal thread spindles via a shaft coupling. On these, cable sleds with corresponding threaded nuts translate the rotational movement into a linear one. These sleds are also mounted on linear guides to absorb any shear forces. At the lower end are the cables attached that lead forward to the respective joints. All bearing points are designed as vacuum-compatible plain bearings.

A great advantage of this cable actuation is that the weight of the structure does not rest solely on the joints and the connecting links, but is compensated to a large extent by the cables. To design the drive unit, the extreme case of a completely horizontally extended arm with a fully loaded payload should always be considered. Here the centre of gravity (COG) of the respective links is furthest away from their axis of rotation and the required cable force $\mathbf{F}_{cable}$ results from the law of gravity:

$$\mathbf{F}_{cable} = \frac{m_{link} \cdot \left\|\mathbf{r}_{cog} \times \mathbf{g}\right\| + \left\|\mathbf{r}_{load} \times \mathbf{F}_{load}\right\| + \left\|\mathbf{r}_{cog} \times \mathbf{F}_{dyn}\right\|}{r_{cable}} \cdot \mathbf{e}_{cable}. \tag{3.1}$$

Where m_{link} is the mass of the link, $\mathbf{r}_{cog}$ the distance between COG and the axis of rotation, $\mathbf{r}_{load}$ the distance between the axis of rotation and the point of application of the additional

load, r_{cable} is the distance between the neutral fibre and the attachment point of the cable in vertical direction and $\mathbf{e}_{cable}$ is the direction of the cable force. The dynamic load $\mathbf{F}_{dyn}$ is negligible for the static design, because since the movements are quasi-static, i.e. very slow, it can be compensated by a small safety factor. In section 3.5, however, it plays a fundamental role in the calculation of the control.

To realise the rotational movements of the links, two types of joints are designed, as seen in fig. 3.8.

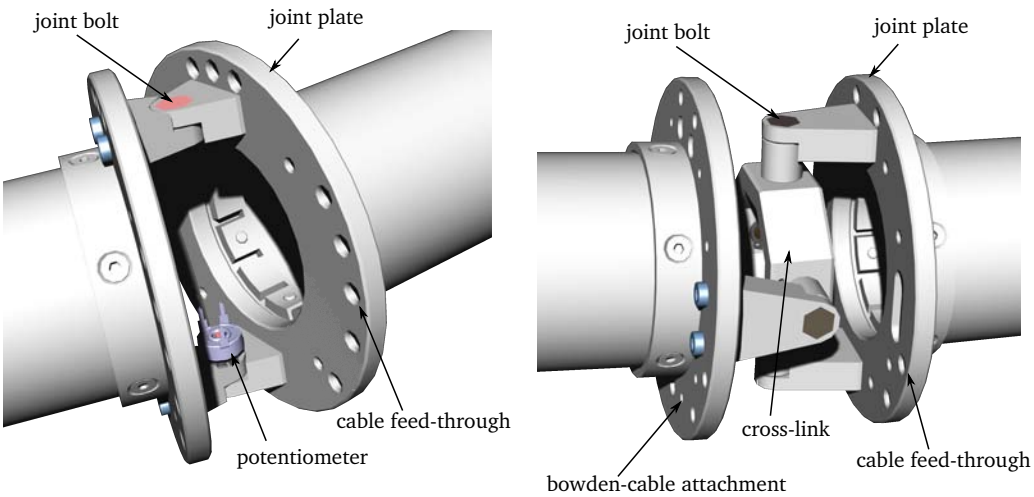

Figure 3.8: 3D-CAD representation of an horizontal joint (left) and an universal joint (right).

Both the horizontal joints and the universal joints consist of joint plates to which the ropes are attached. The former require two ropes and thus also two actuators in order to perform a relative movement around their axis. The universal joints are built in a cross structure and therefore require three ropes or actuators to operate in both DOF. Vacuum-compatible potentiometers are mounted on each axis to measure the angles of rotation. The rigid connecting parts are designed as tubes through which all electronic components are routed.

The current design only provides for active joints. In order to achieve the required freedom of movement, each of these would have to be able to map an angle of ±90°. However, as experiments by HORIGOME AND ENDO [24] show, curvature of drive cables under load must be limited. Therefore, the design is changed so that a segment consists of four links. These are coupled to each other with Bowden cables, which guarantees uniform bending with a maximum angle of rotation of ±22.5° for each axis.

3.5 Kinematics and Control

The most important task in the design of a robot is the precise description of its kinematics. This is essential both for the calculation of the forces that occur and for the design of the control system. Since the concept at hand is a hyperredundant robot, difficulties arise in classical kinematic analysis.

First, the geometric spaces that map onto each other must be defined. The angles of the motors are controlled and regulated. The spindles translate the rotations into linear movements and thus change the length of the cables that exit the actuator box. This relative movement in turn ensures that the joints rotate around their axes. Finally, these movements are mapped onto the end-effector pose. All this is illustrated in fig. 3.9.

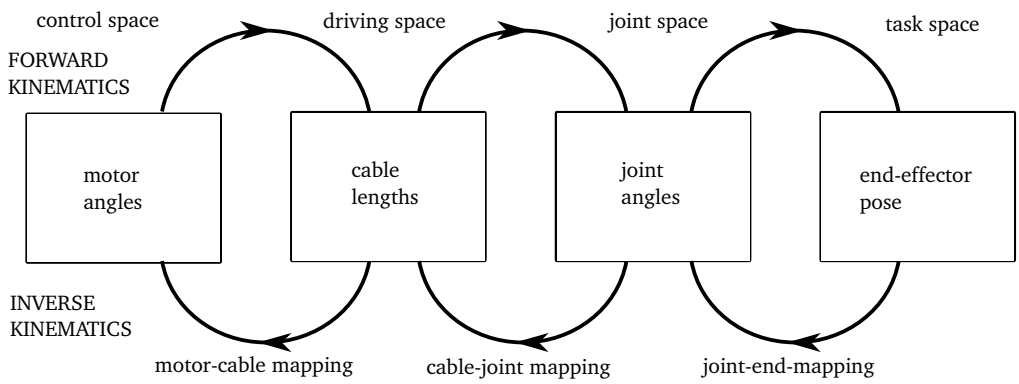

Figure 3.9: Relationships between the geometric spaces.

The upper path symbolises forward kinematics, while the lower path shows inverse kinematics. The former are to be computed first.

3.5.1 Forward kinematics

In forward kinematics, the end-effector pose is calculated with the inputs, in this case the motor angles, already known.

In order to map the change in motor angle $\Delta\phi_{k,n}$ to the change in cable length $\Delta L_{k,n}$, knowledge of the gear ratio i and the pitch of the thread of the spindle $s_{spindle}$ is required:

$$\Delta L_{k,n} = \frac{\Delta\phi_k s_{spindle}}{2\pi i}. \tag{3.2}$$

For the translation of the cable lengths into the joint angles, the horizontal and the universal joints must be considered explicitly. Here, fig. 3.10 provides support.

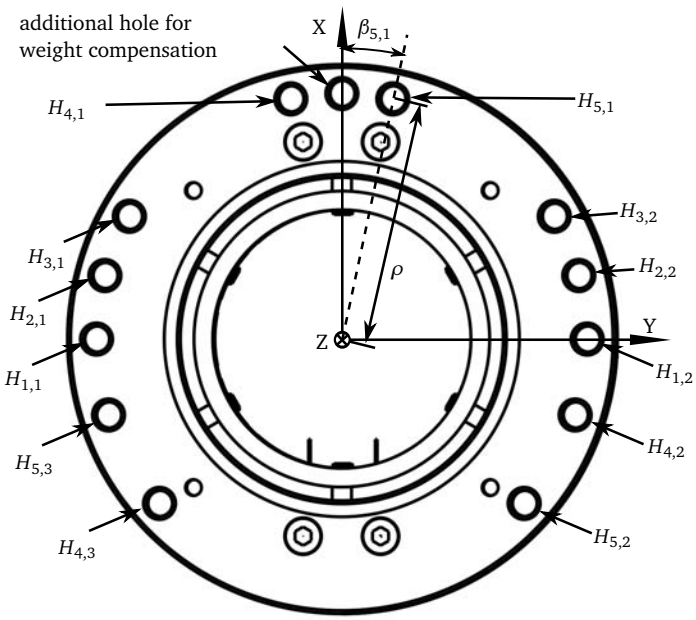

Figure 3.10: Arrangement of the cable ducts.

The cables necessary for the horizontal movement of the first three segments are attached to the holes $H_{k,n}$ with $k \in [1,3]$ and $n \in [1,2]$ arranged opposite to each other. The universal joints require three cables each, which are led through the holes $H_{k,n}$ with $k \in [4,5]$ and $n \in [1,3]$. Since the segments consist of four joints each, $\Delta L_{k,n}$ is divided accordingly among all four links. The following relationship holds only for the horizontal joints:

$$\Delta L_{k,1} = -\Delta L_{k,2} \qquad k \in [1,3]. \tag{3.3}$$

In order to determine the necessary relative movement of the cables for setting an angle, one can make use of the tool of homogeneous transformation. The transformation matrix ${}^{j}\boldsymbol{A}_i$ can be written as follows:

$${}^{j}\boldsymbol{A}_i = \begin{bmatrix} {}^{j}\boldsymbol{R}_i & {}^{j}\boldsymbol{P}_i \\ \boldsymbol{0} & 1 \end{bmatrix}, \tag{3.4}$$

where ${}^{j}\boldsymbol{R}_i \in \mathrm{R}^{3\times 3}$ and ${}^{j}\boldsymbol{P}_i \in \mathrm{R}^3$ are, respectively, the rotation matrix and the position vector. This transformation matrix is used to transfer vector-valued quantities from the coordinate system i into the system j. The standard operations of rotation $Rot()$ and tanslation $Trans()$ are used for this purpose. With the distances between the respective joint plates $2d_{hor}$ and $2d_{uni}$, and the respective angles of rotation about the horizontal Y-axis ψ and the vertical X-axis ζ, the following transformations result:

$$\begin{aligned} \text{horizontal: } {}^{j}\boldsymbol{A}_i &= Trans(0,0,d_{hor})\,Rot(X,\zeta)\,Trans(0,0,d_{hor}) \\ &= \begin{bmatrix} 1 & 0 & 0 & 0 \\ 0 & c_\zeta & -s_\zeta & -s_\zeta d_{hor} \\ 0 & s_\zeta & c_\zeta & c_\zeta d_{hor} + d_{hor} \\ 0 & 0 & 0 & 1 \end{bmatrix}, \end{aligned} \tag{3.5}$$

$$\begin{aligned} \text{universal: } {}^{j}\boldsymbol{A}_i &= Trans(0,0,d_{uni})\,Rot(X,\zeta)\,Rot(Y,\psi)\,Trans(0,0,d_{uni}) \\ &= \begin{bmatrix} c_\psi & 0 & s_\psi & s_\psi d_{uni} \\ s_\zeta s_\psi & c_\zeta & -s_\zeta c_\psi & -s_\zeta c_\psi d_{uni} \\ -c_\zeta s_\psi & s_\zeta & c_\zeta c_\psi & c_\zeta c_\psi d_{uni} + d_{uni} \\ 0 & 0 & 0 & 1 \end{bmatrix}, \end{aligned} \tag{3.6}$$

where $c_\zeta = \cos(\zeta), s_\zeta = \sin(\zeta), c_\psi = \cos(\psi)$, and $s_\psi = \sin(\psi)$.

The positions of the holes in the local coordinate system can be obtained from fig. 3.10 to

$$\mathbf{H}_{k,n} = \begin{bmatrix} s_{\beta_{k,n}}\rho \\ c_{\beta_{k,n}}\rho \\ 0 \\ 1 \end{bmatrix}. \tag{3.7}$$

Together with eq. (3.5), the necessary change of cable lengths for the horizontal joints $k \in [1,3]$ can be determined as follows:

$$\begin{aligned} l\left(\Delta\zeta_k, \Delta\psi_k = 0, \beta_{k,n}\right) &= \left\| {}^{I}\boldsymbol{A}_J^J \boldsymbol{H}_{k,n} - {}^{I}\boldsymbol{H}_{k,n} \right\| \\ &= \left(\left(c_\zeta c_{\beta_{k,n}}\rho - c_{\beta_{k,n}}\rho - s_\zeta \frac{d_{hor}}{2} \right)^2 \right. \\ &\quad \left. + \left(s_\zeta c_{\beta_{k,n}}\rho + c_\zeta \frac{d_{hor}}{2} + \frac{d_{hor}}{2} \right)^2 \right)^{1/2} = l_{k,n}. \end{aligned} \tag{3.8}$$

This can be solved analytically by including eq. (3.3). For the sake of clarity, however, this will not be included here. A similar approach can be taken for the universal joints $k \in [4,5]$:

$$\begin{aligned} l\left(\Delta\zeta_k, \Delta\psi_k, \beta_{k,n}\right) &= \left\| {}^I\boldsymbol{A}_J^J \boldsymbol{H}_{k,n} - {}^I\boldsymbol{H}_{k,n} \right\| \\ &= \left(\left(\frac{d_{uni}}{2} s_\psi + \rho c_\psi c_{\beta_{k,n}} - \rho c_{\beta_{k,n}} \right)^2 \right. \\ &\quad + \left(\rho c_{\beta_{k,n}} s_\zeta s_\psi + \rho c_\zeta s_{\beta_{k,n}} - \frac{d_{uni}}{2} s_\zeta c_\psi - \rho s_{\beta_{k,n}} \right)^2 \\ &\quad \left. + \left(\rho s_\zeta s_{\beta_{k,n}} - \rho c_{\beta_{k,n}} c_\zeta s_\psi + d c_\zeta c_\psi + \frac{d_{uni}}{2} \right)^2 \right)^{1/2} = l_{k,n}. \end{aligned} \tag{3.9}$$

Additionally, it has to be considered that the total length of the cable $L_{k,n}$ with $k \in [2,5]$ is not only influenced by the joints of segment k, but also by segments 1 to $k-1$. eqs. (3.8) to (3.9) can then be added to $\Delta L_{k,n}$ as follows:

$$\Delta L_{k,n} = 4\left(l_{k,n} + l\left(\Delta\zeta_{k-1}, \Delta\psi_{k-1}, \beta_{k,n}\right) + \cdots + l\left(\Delta\zeta_1, \Delta\psi_1, \beta_{k,n}\right)\right). \tag{3.10}$$

Equation (3.9) cannot be solved analytically because three equations, namely the cable lengths $l_{k,1}$, $l_{k,2}$ and $l_{k,3}$, for the determination of the respective unknowns ψ and ζ are present and the system of equations is thus overdetermined. To solve this problem, a numerical solution with the help of pseudo-inverse Jacobian matrices is possible. This procedure, also used by PENG ET AL. [43] among others, is adapted to the kineamtic analysis of IVAR.

First, the differential equations resulting from eq. (3.9) must be established:

$$\begin{bmatrix} dl_{k,1} \\ dl_{k,2} \\ dl_{k,3} \end{bmatrix} = \boldsymbol{J}_d \begin{bmatrix} d\zeta \\ d\psi \end{bmatrix}, \tag{3.11}$$

$$\boldsymbol{J}_d = \begin{bmatrix} \frac{\partial l_{k,1}}{\partial \zeta} & \frac{\partial l_{k,1}}{\partial \psi} \\ \frac{\partial l_{k,2}}{\partial \zeta} & \frac{\partial l_{k,2}}{\partial \psi} \\ \frac{\partial l_{k,3}}{\partial \zeta} & \frac{\partial l_{k,3}}{\partial \psi} \end{bmatrix}, \tag{3.12}$$

with $\boldsymbol{J}_d$ as the Jakobian matrix. Since this is not invertible, due to its non symmetric dimension, the pseudo inverse $\boldsymbol{J}_d^+$ is used:

$$\begin{bmatrix} \Delta\zeta \\ \Delta\psi \end{bmatrix} = \boldsymbol{J}_d^+ \begin{bmatrix} \Delta l_{k,1} \\ \Delta l_{k,2} \\ \Delta l_{k,3} \end{bmatrix}, \tag{3.13}$$

$$\boldsymbol{J}_d^+ = (\boldsymbol{J}_d)^{\mathrm{T}} \cdot \left(\boldsymbol{J}_d \boldsymbol{J}_d^{\mathrm{T}}\right)^{-1}. \tag{3.14}$$

The pseudo inverse $\boldsymbol{J}_d^+$ is not unique and ensures that one degree of freedom of the original Jacobian matrix is fixed, translating in this case a three-dimensional problem into the two-dimensional one. In the field of structural dynamics, these pseudo inverses are mainly used in static condensation.

Starting from a predefined initial value for the angles ζ and ψ and a the cable length obtained from the motor-cable mapping, it can be iterated towards a numerically correct solution according to the following algorithm.

Data: desired cable length l_d
Result: solution for $\begin{bmatrix} \Delta\zeta & \Delta\psi \end{bmatrix}^T$
initialisation;
$\begin{bmatrix} \Delta\zeta & \Delta\psi \end{bmatrix}^T = \begin{bmatrix} \Delta\zeta & \Delta\psi \end{bmatrix}_0^T$;
$j = 0$; $j_{max} = 1000$; $\epsilon = 10^{-3}$;
solutionFound = false;
while *solutionFound != true* **do**
  calculate l_j according to eq. (3.9);
  $\Delta l_j = l_d - l_j$ **if** *norm*$(\Delta l_j \geq \epsilon)$ **then**
    calculate $\boldsymbol{J}_d$ according to eq. (3.12);
    $\begin{bmatrix} \Delta\zeta & \Delta\psi \end{bmatrix}_{j+1}^T = \boldsymbol{J}_d^+ \cdot \Delta l_j$;
    $\begin{bmatrix} \zeta & \psi \end{bmatrix}_{j+1}^T = \begin{bmatrix} \zeta & \psi \end{bmatrix}_j^T + \begin{bmatrix} \Delta\zeta & \Delta\psi \end{bmatrix}_{j+1}^T$;
    $j = j + 1$;
    if $j < j_{max}$) **then**
      return;
    else
      abort;
    end
  else
    solutionFound=true;
    return;
  end
end

Algorithm 1: Algorithm for the numerical solution to the joint angles.

The resulting joint angles are acceptably accurate and serve as input variables for the calculation of the end-effector pose in the following steps.

To complete the calculation of the forward kinematics, the end effector pose must be determined from the joint angles.

According to Craig [11] the following steps must be worked through in order to set up the Denavit-Hartenberg Parameter (D-H Parameter).

1. Enumerate the links beginning with 1 as the first mobile link in the chain, and end with n as the last mobile link. The fixed base will be enumerated with a 0.

2. Enumerate each joint beginning with 1 as the correspondent to the first DOF and ending with n.

3. Localise the axis of each joint. If it is rotational, the axis will be located around the pivot line. If it is prismatic, the axis will be located along the displacement.

4. For a given k from 1 to n put the axis $\mathrm{Z_k}$ over the joint k.

5. Put the origin of the system in the base as S_0 in any point of the axis Z_0. The axis X_0 and Y_0 will be set following the right-hand rotation rule to obtain $\mathrm{Z_0}$.

6. For k from 0 to $n-1$, put the system $S_{\mathrm{k+1}}$ in the intersection of the axis $\mathrm{Z_{k+1}}$ with the perpendicular line of both $\mathrm{Z_k}$ and $\mathrm{Z_{k+1}}$. If both axis crossed, $\mathrm{S_{k+1}}$ would be located in

the intersection point. If both axis were parallel, S_{k+1} would be located in the joint $k+1$.

7. Put X_k in the perpendicular line of both Z_k and Z_{k+1}.
8. Put Y_k so it follows the right-hand rule for rotations with X_k and Z_k.
9. Obtain θ_k as the angle needed to rotate around Z_k so X_{k-1} and X_k are parallel.
10. Obtain d_k as the distance along Z_k that would be needed to move S_{k-1} so X_k and X_{k-1} are aligned.
11. Obtain a_k as the distance along X_k in order to make the origin of S_k and S_{k+1} coincident.
12. Obtain α_k as the angle around X_k needed so the system S_k is totally coincident with S_{k+1}.
13. Obtain the transformation matrices ${}^{k-1}\boldsymbol{A}_k$, where:

$$ {}^{k-1}\boldsymbol{A}_k = \begin{bmatrix} c_{\Theta_k} & -s_{\Theta_k} & 0 & a_{k-1} \\ s_{\Theta_k} c_{\alpha_{k-1}} & c_{\Theta_k} c_{\alpha_{k-1}} & -s_{\alpha_{k-1}} & -s_{\alpha_{k-1}} d_k \\ s_{\Theta_k} s_{\alpha_{k-1}} & c_{\Theta_k} s_{\alpha_{k-1}} & c_{\alpha_{k-1}} & c_{\alpha_{k-1}} d_k \\ 0 & 0 & 0 & 1 \end{bmatrix}. \tag{3.15} $$

14. Obtain the transformation matrix that relates the base with the tip of the robot.

$$ \boldsymbol{T} = {}^{0}\boldsymbol{A}_1 {}^{1}\boldsymbol{A}_2 \ldots {}^{n-1}\boldsymbol{A}_n. \tag{3.16} $$

15. The matrix T defines the orientation and the position of the tip of the robot referred to the base expressed as the n joint variables.

Figure 3.11 shows the necessary coordinate systems.

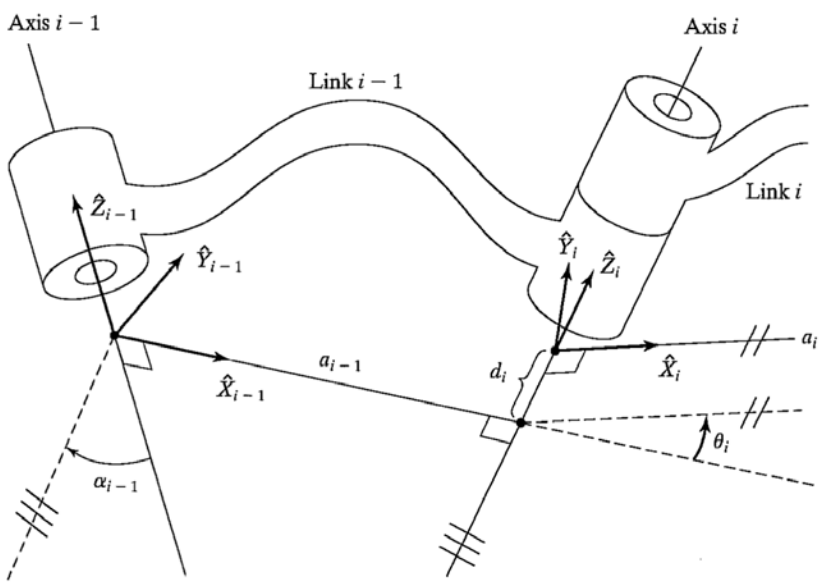

Figure 3.11: Illustration of the axes for determining the D-H Parameter [11].

The resulting D-H Parameter for IVAR are shown in the table 3.1.

Axis k	a_{k-1} (mm)	$\alpha_{k-1}(°)$	d_k (mm)	$\Theta_k(°)$
1	0	0	d_1	0
2	length of feeding link	90	0	Θ_2
3 - 5	300	0	0	Θ_2
6 - 9	300	0	0	Θ_3
10 - 13	300	0	0	Θ_4
14	300	0	0	Θ_5
15	0	-90	0	Θ_6
16	300	0	0	Θ_6
17	0	90	0	Θ_5
18	300	0	0	Θ_5
19	0	-90	0	Θ_6
20	300	0	0	Θ_6
21	0	90	0	Θ_5
22	300	0	0	Θ_8
23	0	-90	0	Θ_7
24	300	0	0	Θ_7
25	0	90	0	Θ_8
26	300	0	0	Θ_8
27	0	-90	0	Θ_7
28	300	0	0	Θ_7
29	0	90	0	Θ_8
30	300	0	0	0

Table 3.1: D-H Parameter of the IVAR.

As can be seen in table 3.1, the DOF Θ_2 to Θ_8 of the individual segments are repeated because the coupling through the bowden cables has already been considered.

By multiplying the transformation matrices according to eq. (3.15), the forward kinematics from the base to the tool can be completely calculated.

3.5.2 Inverse kinematics and control

The inverse kinematics tries to calculate corresponding inputs, in this case rotation angles of the motors, in order to achieve fixed poses of the end effector. For mapping the cable-joint kinematics, this has already been done in eqs. (3.8) to (3.9).

Also eq. (3.2) is easily invertible to

$$\Delta\phi_{k,n} = \frac{2\pi i \Delta L_{k,n}}{s_{spindle}}. \tag{3.17}$$

In contrast, when calculating the end-effector joint kinematics, the same problem arises as before with the cable-joint mapping: due to the redundancies of the joint axes, the system is overdetermined and thus the Jacobian matix $\boldsymbol{J}_X$ is also not invertible. Again, to a first approximation, a numerical, iterative method can be used to solve the problem, which is very similar to Algorithm 1 and has been validated by LIU ET AL. [32], among others.

Since this numerical solution means a considerable computational effort, these calculations are to be carried out offline and stored discretised with the required step size in a lookup table for the control of IVAR. This enables real-time operation and a kinematic feedforward control can be implemented. The actual control approach consists of an online calculation of

the necessary cable movements $l_{dk,n}$ or the motor angles according to the angular positions of the respective joints known from the lookup table. Therefore, the following control law is applicable to calculate a control parameter $u_{k,n}$ for every motor:

$$u_{k,n} = K_P\left(l_{dk,n} - l_{k,n}\right) + K_I \int_0^t \left(l_{dk,n} - l_{k,n}\right) dt + K_D\left(\frac{dl_{dk,n}}{dt} - \frac{dl_{k,n}}{dt}\right). \tag{3.18}$$

The parameters for the proportional element K_P, the integration element K_I and the differential element K_D of the PID controller must be tuned manually before operation. Appropriate tools from the motor manufacturers should be used for this. The IVAR is therefore controlled according to the scheme in fig. 3.12.

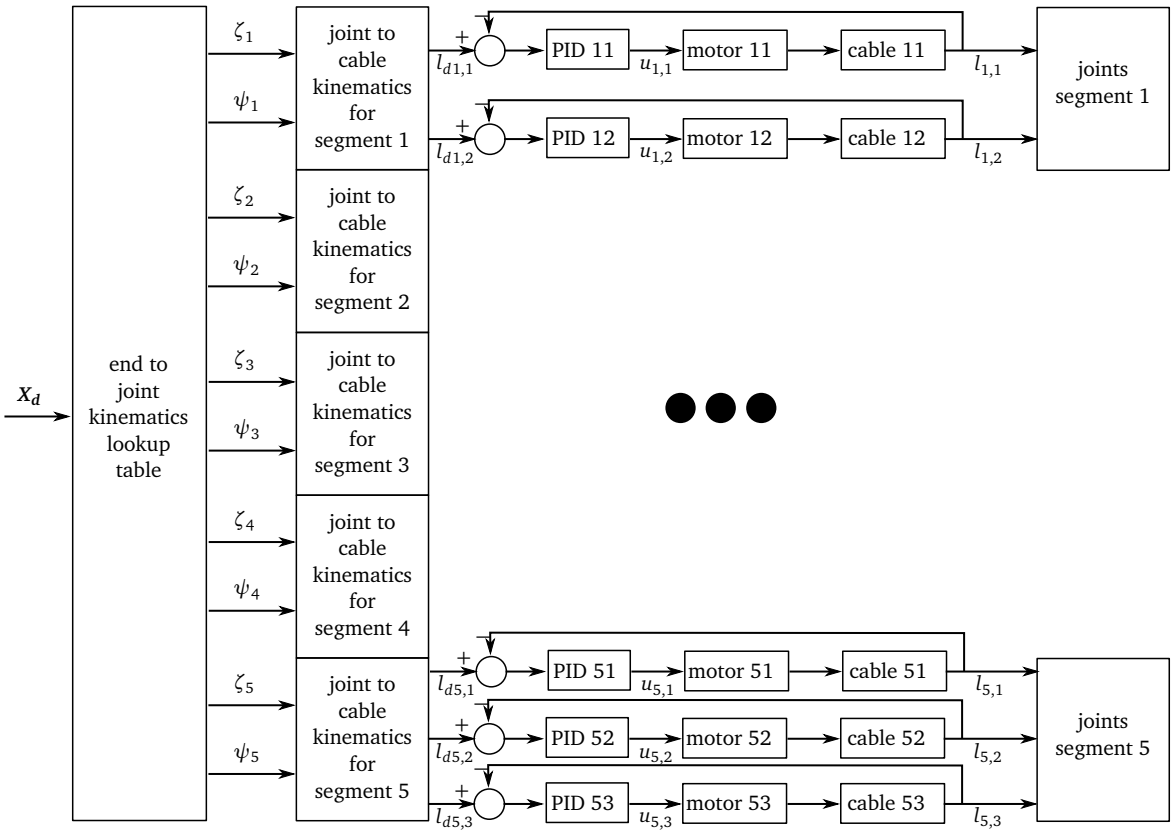

Figure 3.12: General Control Scheme.

For this control principle, the encoders of the motors serve as the stand-alone sensors. The potentiometers on the individual joints are only used to synchronise the axes. For further development, however, these can also be actively included in the control and thus possibly lead to a higher precision in a dual control loop.

3.6 Final Concept

At this point, the concept should be briefly summarised once again. After defining the requirements for a remote handling arm for ASDEX Upgrade, the basic development parameters were set. The geometric constraints imposed by the sequence of inspection movements limit the maximum length of the successively inserted segments to 1.2 m whereby a total length of 6 m may be achieved and a maximum diameter of 89 mm may not be exceeded.

Since the structure resembles a cantilever arm, the decision was made to pursue a decentralised actuation concept in which all drives are located in a motor box and the movements are transferred to the joints at the front by means of cables. This necessitates another modification to the system, because the cable design limits the maximum joint angle to 22.5°, which violates the achievable workspace requirement. For this reason, the five segments are not to be designed rigidly, but are to be subdivided again into four links, which are coupled by Bowden cables. A robot with seven rotational and one translational DOF is designed as shown in fig. 3.13.

Figure 3.13: 3D-CAD representation of the IVAR concept.

The illustration shows the general design as well as a rigid feed tube and a gripping mechanism. The former has to be reconsidered in a further evaluation, as it has not yet been determined how the vacuum housing has to look concretely until the end of the project. Details on this will be taken up again in chapter 5. The gripper is representative of the tools that can be used. Such a tool was also designed for the demostrator as described in chapter 4.

Chapter 4

Proof of Concept: the IVAR Demonstrator

In order to verify the assumptions involved in chapter 3, the following chapters describe the construction of a demonstrator. This primarily serves the domain of robotics and is intended to show that the mechanical construction is sufficient for the purpose of inspection. To this end, the development and construction of the necessary hardware, i.e. the mechanical and the electronic components, is first described. In order that the control system can also be checked to a certain extent, an initial programme sequence is developed in section 4.2. This also verifies the adequate design of the drives. Furthermore, the experiments necessary for the proof of concept are described.

The IVAR demonstrator is depicted in fig. 4.1.

Figure 4.1: Setup of the IVAR demonstrator.

As the figure shows, this consists of a linear axis, an actuator box that is not fully equipped, a horizontally movable segment and a segment with universal joints. Every segment consists of four links, each 300 mm long. In addition, the demonstrator has a toolhead that is equipped with a gripper and a camera. The most important parameters are summarised in table 4.1.

Property	Value	Unit
DOF	4	-
Link diameter	85	mm
Link length	300	mm
Number of links per segment	4	-
Number of horizontal segments	1	-
Number of universal segments	1	-
Number of drives	5	-
Maximum joint angle	22.5	°
Length of linear axis	2000	mm
Mass of cantilever structure	4100	g

Table 4.1: Main properties of the IVAR demonstrator.

4.1 Hardware

Based on the concept for IVAR designed in chapter 3, the hardware components are now developed with the help of Computer Aided Design (CAD), as shown in fig. 4.2.

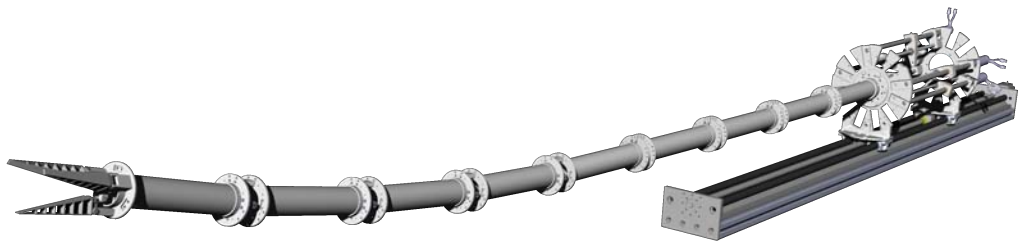

Figure 4.2: 3D-CAD representation of the IVAR demonstrator.

The function of the joints is crucial, which, like all other components, were designed in CATIA V5R21 [10] and derived for the production drawings. The parts with the assumed highest load are additionally checked using FEM in Ansys Mechanical [2], a programme for structural analysis. Furthermore, the design of the actuation unit and the linear axis designed exclusively for the demonstrator are described. The bridge from the mechanical to the electronic parts is built by the toolhead, for which a gripper with camera was constructed for demonstration purposes only. The control architecture as well as the wiring and power supply is covered in section 4.1.6.

4.1.1 Horizontal joints

As fig. 4.3 shows, the first segment after the actuator box consists of four links connected by joints. These correspond to the horizontal design shown in fig. 3.8. While titanium was initially discussed as the main material for the links, aluminium was ultimately chosen due to its lower density and price. A FEM examination of the structure confirms sufficient strength, even if a load-bearing rope should unexpectedly break. The axle pins as well as the sliding washers between the joint bars are made of tin bronze to reduce friction. All screws used are made of stainless steel. The materials used were selected for their vacuum suitability and always represent a compromise between strength and mass. The joint plates are attached to the rigid tubes with six countersunk screws and inlays on the inside. This simplifies the

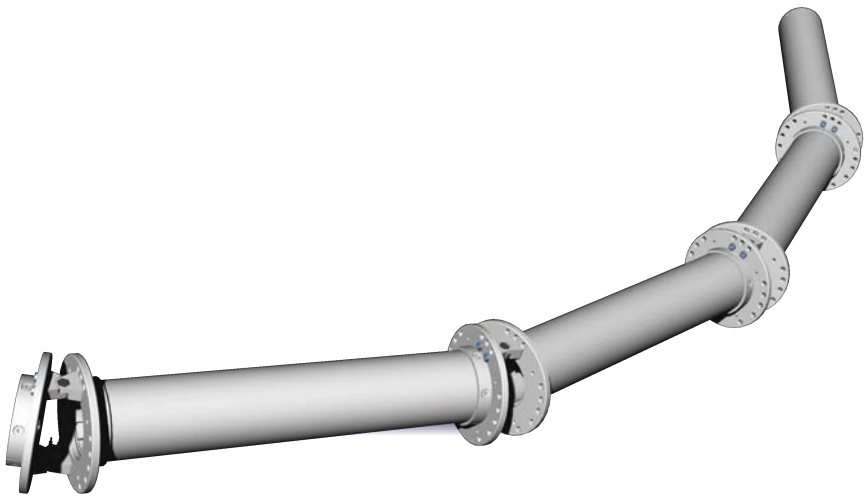

Figure 4.3: 3D-CAD representation of a segment with horizontal joints.

assembly process compared to welded joints and makes modular construction possible. Care has been taken not to create any sharp edges in the cable holes on the joint plates so that the cables are not damaged during operation. Two Bowden cables for each link with Bowden cable sheaths made of non-coated stainless steel couple the four joints together to ensure uniform angles.

4.1.2 Universal joints

For the second segment, as shown in fig. 4.4, basically the same considerations apply as in section 4.1.1. However, its joints rotate around the horizontal as well as the vertical axis. Thus, two DOF are served by this segment. The main element is the cross link, which consists of an octagonal ring with four sockets arranged at right angles. The axles are also made of tin bronze to ensure that the aluminium joint bars do not seize up. Like the horizontal joints, the universal joints were also produced on modern CNC milling machines and lathes by skilled labour.

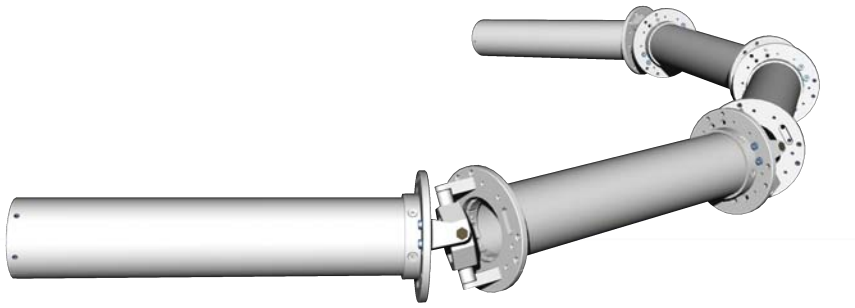

Figure 4.4: 3D-CAD representation of a segment with universal joints.

4.1.3 Actorbox and cables

The drives are housed in a barrel-shaped actuator box. This consists of two aluminium retaining plates into which the drive units are screwed with an exact fit. These units consist of two bearing blocks made of aluminium, a linear guide made of stainless steel, and a spindle with trapezoidal thread TR16x3. This is driven by Brushless Direct Current (BLDC) servo motors (Maxon EC-max 30) via a planetary gear (Maxon GP32C, $i = 111 : 1$). A polymer-damped shaft coupling takes over the power transmission. The cables are attached to aluminium cable slides that move along the linear guide driven by a trapezoidal thread nut. All bearings and also the spindle nut are made of vacuum-compatible polymers (IGUS iglidur X [26]) designed for dry running. The actor box is shown in fig. 4.5.

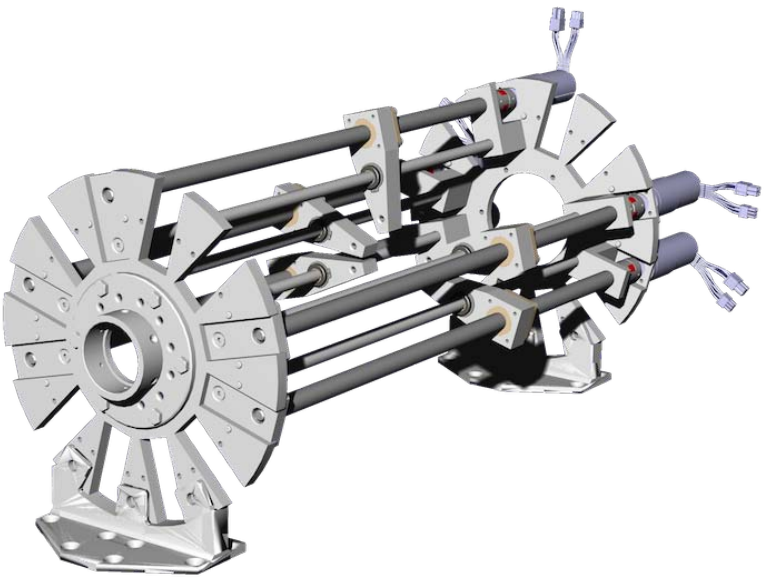

Figure 4.5: 3D-CAD representation of the actorbox.

It should be noted that the motors used for the demonstrator are not suitable for vacuum operation, as the delivery time of the Maxon EC-4pole30 designed for operation in high vacuum would have exceeded the processing time for the master's thesis, and the standard models also meet the requirements for the demonstrator.

For the actuation there remain the ropes used: both for the Bowden cables (diameter 1.5 mm) and for the actuation cables (diameter 3 mm) ropes made of Dyneema SK78 [53] were used. This material is composed of UHMWPE fibres and offers equivalent strength at a seventh of the mass compared to a stainless steel rope of the same diameter. Since one of the main tasks of the design is the lightweight construction of the arm, these ropes were preferred. A manufacturer's specification for vacuum suitability is not available, so the outgassing behaviour was investigated. At 10^{-6} mbar and 80 °C, no substances that could contaminate the reactor outgas, which allows the ropes to be used for IVAR at room temperature of around 30 °C inside ASDEX Upgrade. An outgassing chamber at the Max Planck Institute was used for the experiment. Since there is a possibility that parts of the polyurethane coating of the ropes may come off, uncoated ropes were specially made for IVAR.

4.1.4 Linear axis

Exclusively for the demonstrator setup, a commercially available linear axis was procured without regard to vacuum suitability, as seen in fig. 4.6.

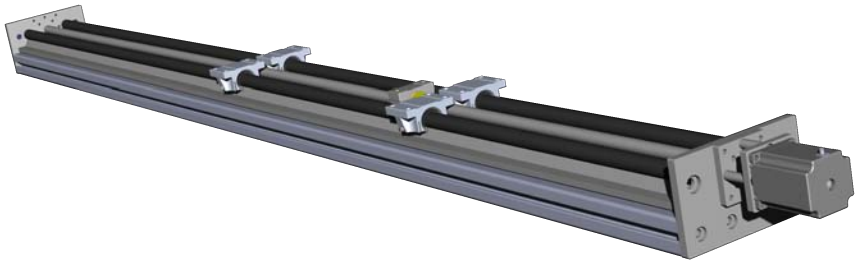

Figure 4.6: 3D-CAD representation of the linear axis.

This 2000 mm long unit consists of a 40 × 160 mm aluminium profile. Attached to this are two bearing plates fitted with a 3200/5200 2RS angular contact ball bearing and a 6200 2RS deep groove ball bearing. The spindle with TR16x4 trapezoidal thread is driven by a NEMA23 stepper motor. The corresponding threaded nut made of gunmetal, which is firmly connected to the actuator box, ensures the translation into a linear movement. Two supported rails of type TBS20 with four corresponding linear bearings of type TBR20UU serve as linear guides. All components are part of the Easy-Mechatronics System 1620A from Dold-Mechatronik [13].

4.1.5 Toolhead

To demonstrate the functionality of the inspection system, a toolhead with gripper and camera was developed for the demonstrator as shown in fig. 4.7.

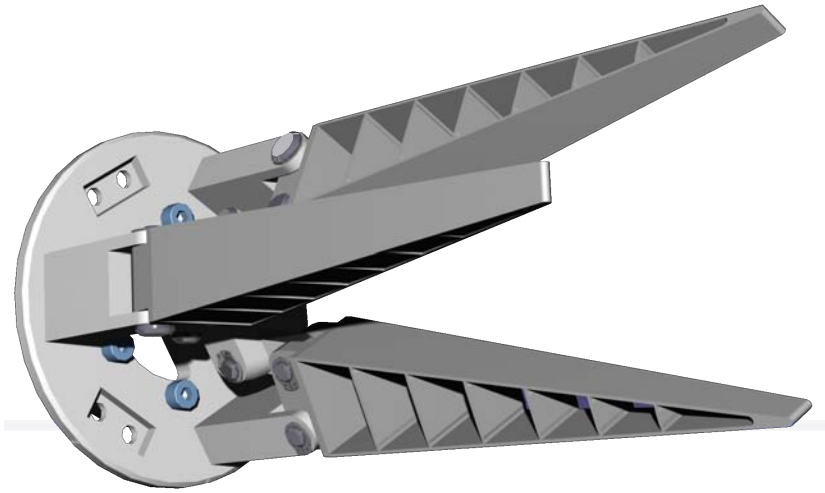

Figure 4.7: 3D-CAD representation of the Toolhead with a three finger gripper.

This unit is also for demonstration purposes only and so is not intended for use in

ASDEX Upgrade. All mechanical parts were additively manufactured with an Ultimaker 5S [54]. Only the gripper fingers are made of nylon and all other parts are made of Chlorinated Polyethylene (CPE). The design of the fingers is based on a popular design for modern soft robotic grippers and is modelled on the structure of the tail fin of a fish [12]. These so-called finray grippers curve around the point where an object exerts force on them and therefore ensure that this object is enclosed. Figure 4.8 demonstrates this principle.

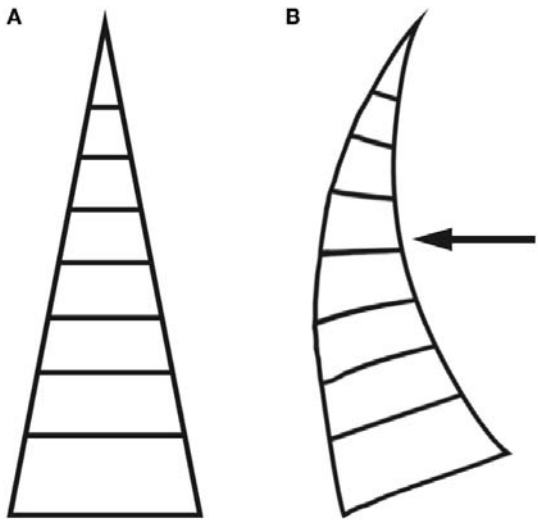

Figure 4.8: Illustration of the finray effect: **A** unloaded condition, **B** from the right a force is applied and the structure bends around the point of application of the force [12].

The advantage of the additively manufactured structure is that solid bearings can be printed in one piece. This saves resources and makes rapid prototyping possible.

A Bowden cable that runs through the entire arm actuates the gripper and is tensioned by a pneumatic cylinder. The cable is attached to a pull plate that ensures the closing of the gripper via a lever structure. Automatic opening is provided by a pre-tensioned spring when the force of the pneumatic cylinder is reduced.

4.1.6 Electronic design

The toolhead provides the appropriate transition to the electronic design, because a camera is also placed on it. For this purpose, an ESP32 microcontroller [15] with a camera module is attached to the gripper. Since this microcontroller has a WiFi module too, the images can be sent to a web server via a User Datagram Protocol (UDP) stream and thus easily viewed via the browser window of a WiFi-capable end device. It is therefore sufficient to supply the ESP32 with power - a data line is not required. The programming is taken up again in section 4.2.

One or respectively two hollow shaft potentiometers (PIHER PTC10 - 10 kΩ) are fitted to all horizontal and universal joints, enabling the joint angles to be determined precisely. In order not to disturb the analogue signals by too long data lines and to reduce the number of cables, microcontrollers (Seeeduino XIAO [49]) for the analogue-digital conversion of the potentiometers of each rotary DOF were built directly into the arm structure. These units offer the possibility to integrate them into a Inter-Integrated Circuit (I^2C) bus system. This means that only two cables (Data and Clock) are needed to transmit data to the master system and makes clean cable management within the arm structure possible.

The motors described in section 4.1.3 are electronically commutated and have one pole pair. Equipped with a Hall sensor and an incremental encoder for speed and angle measurement, the drives are controlled and supplied with power by two multi-axis controllers (Maxon MINIMACS6). Each of these can control a maximum of four BLDC servo motors up to a total continuous power consumption of 540 W. In this case, the drives of each segment are connected to a separate controller. In order to also ensure synchronisation between these, they are integrated into a field bus system: in a daisy-chain topology, the two slaves are connected to a master using Ethernet for Control Automation Technology (EtherCAT). It is designed for motion control applications, i.e. applications with very short cycle times where synchronicity, simultaneity and cycle fidelity are crucial [16]. The master system in this network is a Raspberry Pi 4 [46]. This single-board computer has enjoyed great popularity for years, both for hobby electronics projects and in industrial applications. Equipped with a quad core 64-bit ARM-Cortex A72 processor running at 1.5 GHz and 1 to 8GB LPDDR4 RAM, it offers enough power for complex kinematics calculations and is capable of running soft real-time applications through an optional Linux realtime kernel. Furthermore, the unit has an I^2C interface, a Fast Ethernet port and is WiFi-capable. The linear axis is controlled directly via the General Purpose Input/Output (GPIO) pins. In this way, the master controller can be optimally integrated into the network structure that has been set up, which can be seen in its entirety in fig. 4.9.

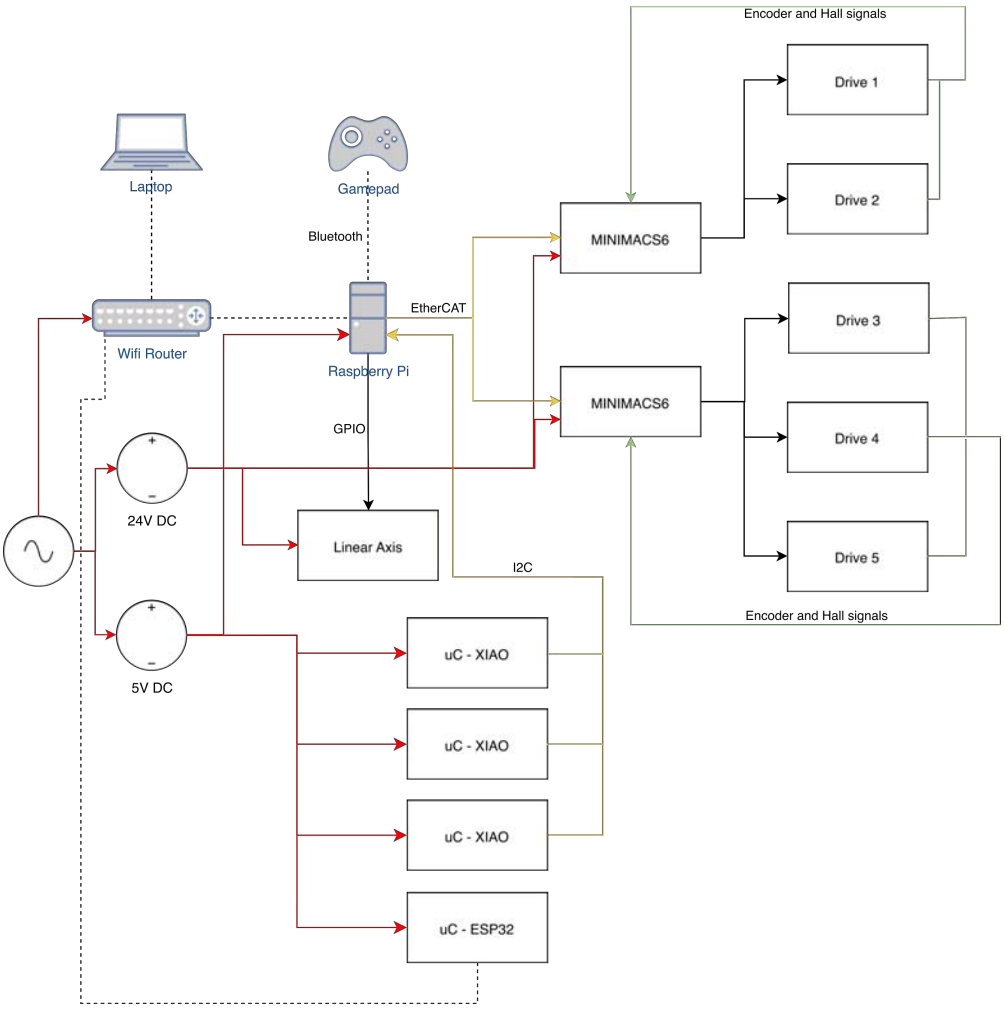

Figure 4.9: IVAR electronic design scheme.

The illustration also shows the power supplies (5 V and 24 V) as well as a laptop as user

interface and a Bluetooth gamepad for user input. This will be discussed further in the next section 4.2.

All non-moving components were professionally mounted on a Polyvinyl Chloride (PVC) plate. A DIN rail was used for this purpose, on which the two power supplies are also attached. The brackets for the Raspberry were again printed out of CPE and an emergency stop switch for interrupting the 230 V AC power supply was also placed on the board. The assembly can be seen in fig. 4.10.

Figure 4.10: View of the electronics assembly.

4.2 Software

After the required hardware has been designed and assembled, the development of the software can continue. In principle, four main components are programmable, which are also shown in fig. 4.9:

- the Raspberry Pi as master controller,
- the Maxon MINIMACS6 as motion controller,
- the Seeeduino XIAO used to process the joint angles measured by the potentiometers,
- the ESP32 and the laptop, which contribute to the user interaction.

In the following sections, the respective software modules are explained and considered in relation to each other. It should be noted at this point that not all modules have been completed at the end of the work due to a lack of time and personnel, and thus there is still a need for further software development. The programme sequences presented therefore serve as a guideline for future design.

4.2.1 Master controller

At the heart of the software is the Robot Operating System (ROS) [48] configured for IVAR. ROS is an open source robotics middleware package. It provides functions similar to an operating system, including hardware abstraction, low-level device control, implementation of

commonly used functions, message passing between processes and package management. It also provides tools and libraries for obtaining, creating, writing and running code on multiple computers. Due to the open source, there is a large community for the development of software components and thus modules, such as for communication with the Bluetooth gamepad, can be adopted without having to develop drivers themselves. The processes or code blocks of a robot are divided into modular *nodes*. These *nodes* communicate with each other via *topics*. Each *node* can *publish* a message on a *topic* or receive a message from it if it is relevant. Then the *node* acts as a *subscriber*. The ROS architecture for IVAR is shown in fig. 4.11.

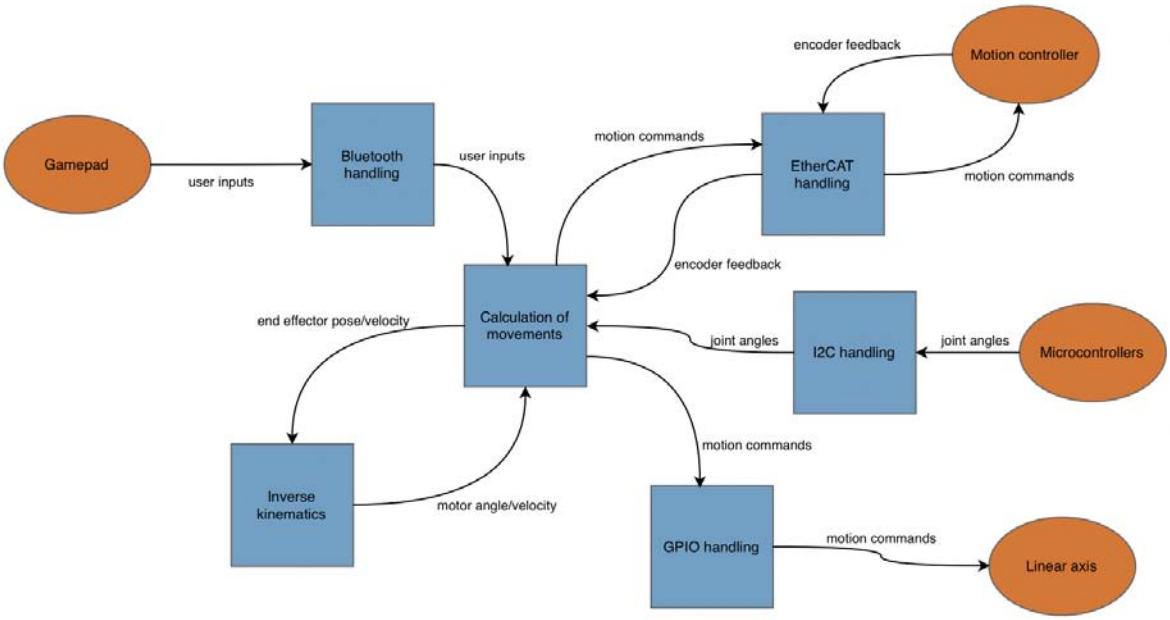

Figure 4.11: Schematic of the ROS architecture for IVAR.

As the graphic shows, the focus is on calculating the necessary movement commands. For this purpose, the user inputs are received via a bluetooth handling node, converted into a desired end effector pose or velocity and transferred to an inverse kinematics node. The necessary motion commands are formed from the results and transferred to the motion controller and the stepper motor of the linear axis via the EtherCAT handling node respectively the GPIO handling node. As an angular reference, the joint angles are queried at continuous intervals via the I^2C handling node using the microcontrollers inside the arm. The individual nodes originate from the main packages of the ROS library or were developed independently in the programming language C/C++.

4.2.2 Motion controller

The two Maxon MINIMACS6 receive their synchronisation and movement commands via the EtherCAT fieldbus from the master controller. The units themselves are also programmable and could also be used as stand-alone solutions. In this case, however, they are programmed with applications that receive the motion commands and take over the direct control of the drives. The programming is done in the Aposs Integrated Development Environment (IDE) [36] provided by Maxon in a C-like programming language. In addition, the Aposs IDE was used to tune the control parameters K_P, K_D and K_I for every drive individually, cf. section 3.5.2.

4.2.3 Joint angle measurement

As described in section 4.2.1, the Raspberry Pi receives the information about the current angular position of the joints via an I^2C interface. The information exchanged is streamed in the form of byte arrays from the three microcontrollers (Seeeduino XIAO) with a cycle time of 10 ms. These units are quite powerful for their size: equipped with a 32bit Cortex M0+ ARM processor (48 MHz) they can read out 14 12bit Analog-Digital Converter (ADC) and process the values. Four of the analogue pins are used to determine the resistance values of the potentiometers of one DOF. The measurement of the angles is carried out redundantly in order to determine measurement inaccuracies and to detect any kinking of the joints due to a rope break. The code running on the units is a simple loop after initialisation, c.f. fig. 4.12, and was also programmed in a C-like language within the Arduino IDE [3].

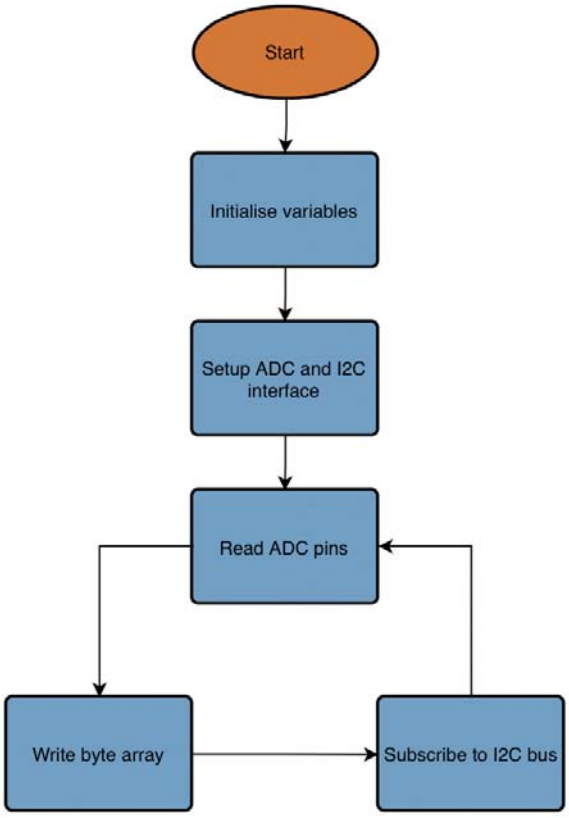

Figure 4.12: Flowchart of the Seeeduinos XIAOs programme.

4.2.4 User interaction

The ESP32 responsible for the visual inspection was also programmed using the Arduino IDE and sends the images captured by the mounted camera to a web server in the form of an UDP stream. This can be received by a WiFi-enabled end device within the same network and played back using a media player or browser application. Most parts of the code were taken from the example programme *CameraWebserver* [20], which Espressif provides for development with ESP32 boards. The exact programme sequence will therefore not be described here. Within the WiFi network set up especially for IVAR, a video stream with 40 frames per second and a XGA resolution (1024x768) could be displayed in the browser window of a Linux laptop.

For user input on the gamepad, the two nodes *teleop_twist_joy* and *joystick_drivers* provided by ROS can be used, which take over both the Bluetooth handling and the evaluation of the potentiometer values of the joysticks.

Chapter 5

Tests and Discussion

In chapter 3, a concept for inspection and remote handling within the vacuum vessel of a Tokamak was developed. For this purpose, requirements were placed on the system, which will be checked for their fulfilment in the following section. Furthermore, chapter 4 describes the construction of a demonstrator, the IVAR demonstrator, whose function will be tested in section 5.2. Finally, it will be discussed to what extent this is sufficient as a proof of concept and which tasks still need to be completed before the construction of a robot that can really be used for remote handling in ASDEX Upgrade can begin.

5.1 Outgasing Tests

The only parts that are not only used for the IVAR demonstrator and do not have a vacuum specification are the ropes made from Dyneema fiber. Therefore, as mentioned in section 4.1.3, mass spectroscopies were determined in an outgassing chamber at the Max Planck Institute, which is shown in fig. 5.1.

Figure 5.1: Oven for vacuum compatibility tests.

After an ultrasonic bath, the cleaned ropes were placed in the oven. Then a vacuum

atmosphere of 10^{-6}mbar was established and the ropes were first heated to 50 °C and in a further measurement campaign to 80 °C. A Residual Gas Analysis (RGA) and pressure measurement were used as diagnostics. In the process, the following mass spectroscopies were made.

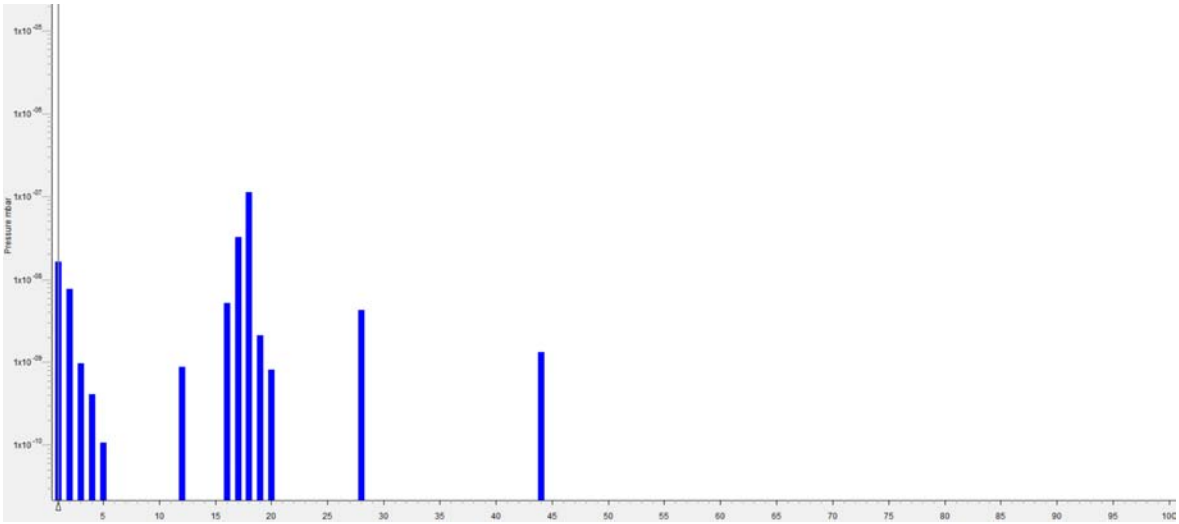

Figure 5.2: Mass spectrum at 50 °C .

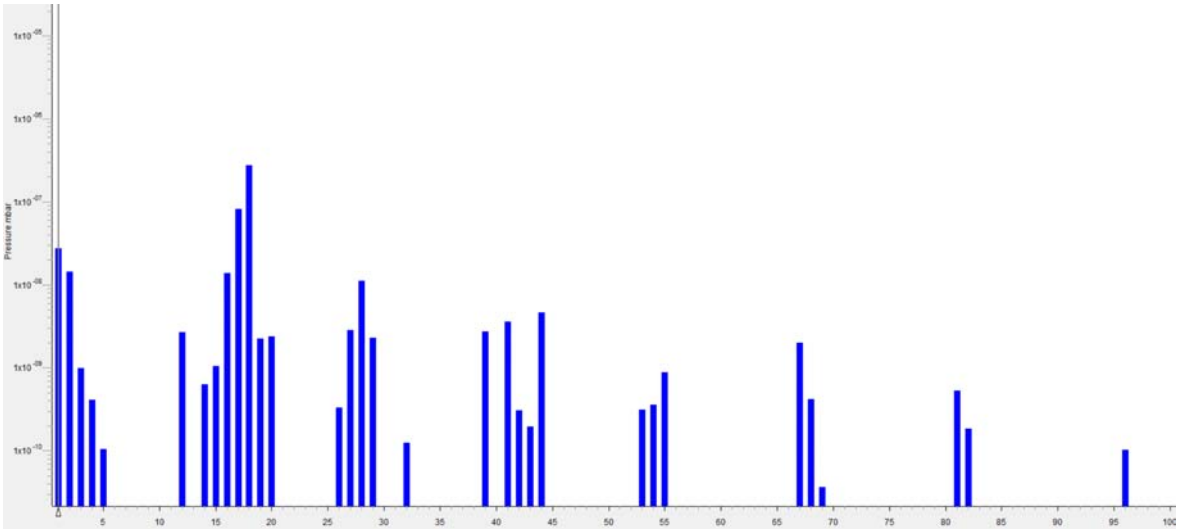

Figure 5.3: Mass spectrum at 80 °C.

The partial pressures of the individual substances are plotted logarythmically in mbar on the vertical axis and their atomic mass in u on the horizontal axis. For operation in ASDEX Upgrade, substances with more than 42 u are of particular importance, as these are mostly hydrocarbon compounds from lubricants or oils that sustainably pollute the vacuum vessel. Attention is also paid to the outgassing of chlorine (35 u) and zinc (65 u). The spectrum at 50 °C shown in fig. 5.2 does not show any substances endangering vacuum operation. In fig. 5.3, some hydrocarbon compounds can be detected, but according to the experts of the vacuum group, they do not yet occur in such quantities that they permanently disturb the vacuum in ASDEX Upgrade. Moreover, the actual operation is supposed to take place at much lower vacuum compatibility requirements (10^{-3}mbar and about 30 °C), which is why the suitability of the Dyneema ropes is hereby confirmed.

5.2 Fuctional Experiments

After setting up the hardware and programming the control software, the first experiments can be carried out. First, the function is checked, as shown in fig. 5.4.

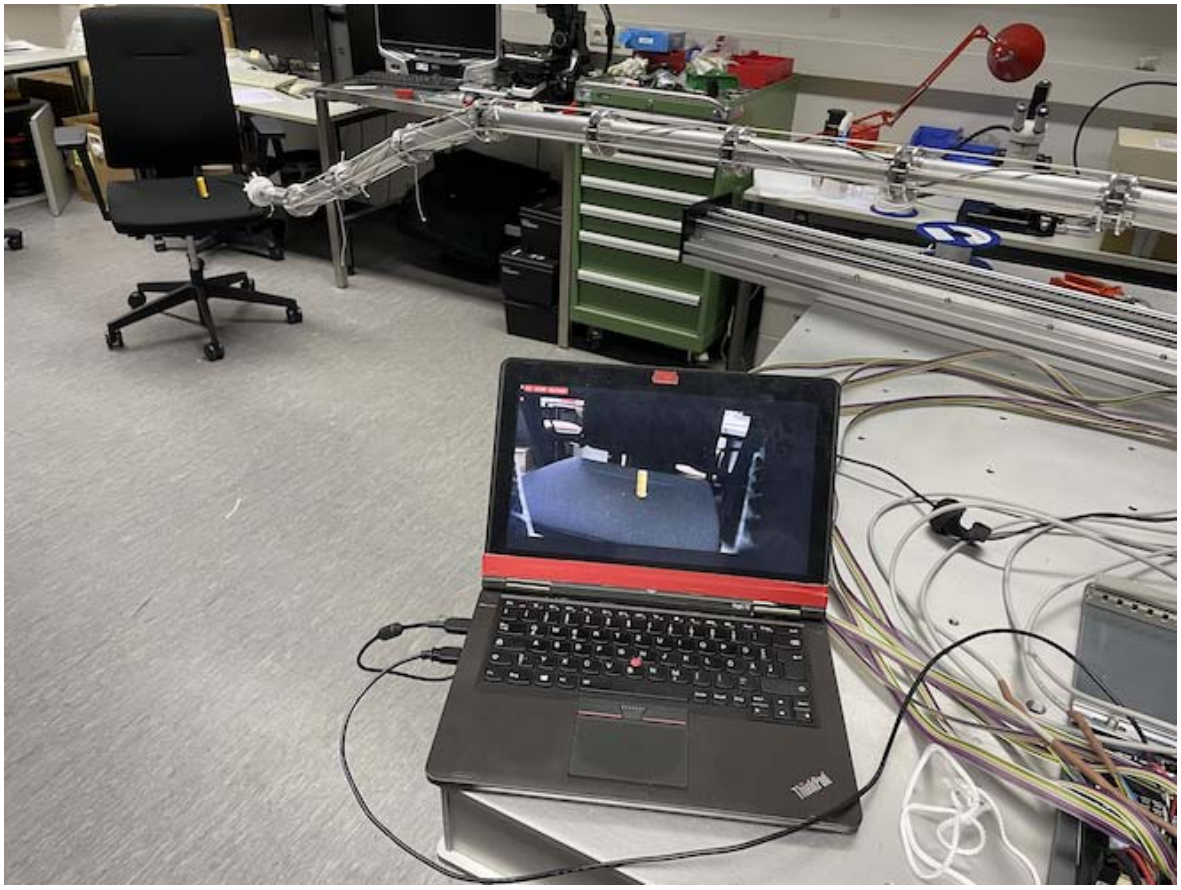

Figure 5.4: Functionality test: control the robot while watching the video stream.

The photo shows how the IVAR demonstrator is used to grasp an object (yellow) on the chair. The user is guided by the video stream displayed on the laptop in the foreground. The linear axis of the robot was moved with a maximum of $8\,\mathrm{mm\,s^{-1}}$ and the joints were rotated with a maximum of $4^\circ\,\mathrm{s^{-1}}$. Without claiming general validity, the control is subjectively perceived as intuitive. Unfortunately, there was not enough time in the last few days of testing to determine the precision and more complex movement sequences. This should be further evluated in later studies.

Furthermore, the structural load capacity of the demonstrator was tested. For this purpose, filament rolls for 3D printing were weighed and attached to the toolhead one after the other. Periodic up and down movements with the arm were then performed in this condition. The first test, also shown in fig. 5.5, was performed with a 1 kg roll. Neither deflection of the links could be detected nor did the motors fail during the execution of the movement. After a slight adjustment of the control parameters, this was also true for the test with a second 1 kg roll (in total 2 kg weight). From this it can be deduced that for use as a gripper arm of heavier objects, a torque-based control must be designed. With the servo motors used, this can be done, for example, by measuring the applied current. Finally, a third roll (in total 3 kg weight) was attached to the arm. While no buckling of the structure occurred here either, the servo motors were no longer able to lift the weight beyond the apex. An evaluation of the controller logs suggests that this was not due to the design of the motors themselves, but to

the dimensioning of the power supply used. For higher loads, it is therefore recommended to use a power supply that can provide more than 10 A at 24 V. In addition, a separate power supply should be used for each controller.

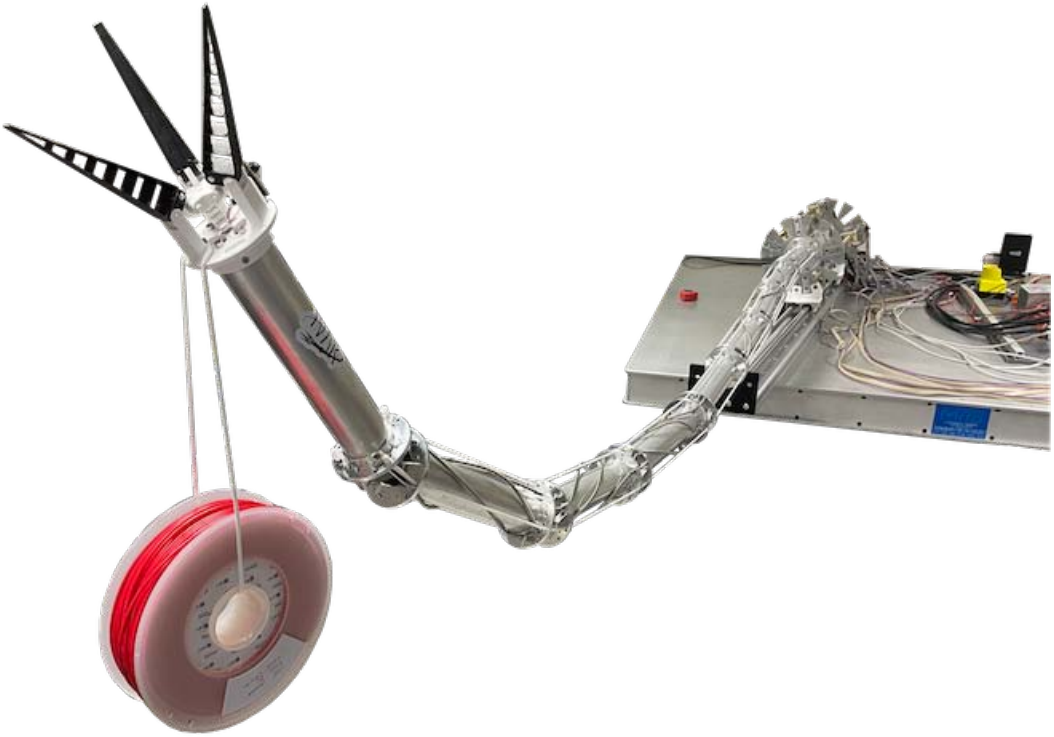

Figure 5.5: The IVAR Demonstrator lifting a 1 kg weight.

5.3 Requirements Validation

The success of the concept development should, as demanded in the Vee model, be based on the requirements established in section 3.2. Their fulfilment will be reviewed below and, if not fully met, commented on.

- "REQ-01: The inspection of the vacuum vessel of ASDEX Upgrade must be possible between plasma shot days"

  fulfilled, but not tested yet.

- "REQ-02: Operation must be possible at an atmospheric pressure of less than 10^{-3}mbar"

  partially fulfilled. Vacuum-compatible servo motors also need to be purchased.

- "REQ-03: The device must be able to be inserted through the port of the midplane manipulator"

  fulfilled.

- "REQ-04: The workspace must be able to map the torus of ASDEX Upgrade"

  fulfilled.

- "REQ-05: The vacuum must not be contaminated"

  partially fulfilled. A vacuum enclosure and pump-out mechanism still need to be designed.

- "REQ-06: The unit must have a payload of at least 2 kg"

  fulfilled.

- "REQ-07: Instruments for inspection (camera, light, gripper) must be able to be attached"

  fulfilled.

- "REQ-08: The device should be modular in terms of usable instruments and future upgrades"

  fulfilled.

- "REQ-09: The travel speed should be greater than or equal to $0.25\,\mathrm{m\,min^{-1}}$"

  fulfilled.

- "REQ-10: The position and orientation of the unit should be verifiable at all times"

  fulfilled.

- "REQ-11: The system should be intuitive to use"

  partially fulfilled. An adequate user interface still needs to be finalised and adapted to IVAR.

- "REQ-12: The system should be able to be stored in the Torus hall when not in use"

  not investigated in detail. So far, no storage site has been identified, nor has an enclosure for storage been designed.

The general concept can therefore be described as proofed. However, the next steps are to develop a vacuum housing to fully meet the requirements. Furthermore, a storage facility and a method for connecting IVAR to ASDEX Upgrade must be identified. Vacuum compatible servo motors have already been selected and need to be purchased and tested. In addition, the software must be finalised and adapted in terms of operability to the wishes of the future maintenance team.

Chapter 6

Summary and Outlook

The purpose of this work was to develop a concept for an inspection robot. This should be able to inspect the inside of the vacuum vessel of the ASDEX Upgrade fusion research experiment and carry out minor maintenance work. In doing so, it should avoid opening the vessel and thus neither break nor contaminate the vacuum atmosphere necessary for plasma operation. ASDEX Upgrade was not prepared for such remote handling, nor are there commercially available robots that can do the job. Similar concepts have been developed for other research projects in the past, but these cannot be adapted to ASDEX Upgrade either. Therefore, using systems engineering methods, a cable-driven, hyperredundant and cantilevered arm was developed that can inspect a half torus of ASDEX Upgrade in a continuous motion. The arm has seven rotational DOF and one translational DOF and can thus perform complex movement patterns. Its 6 m cantilever structure places considerable stress on the components used. Therefore, extreme lightweight construction was taken into account in the design and modern engineering principles were observed. The special structure of a hyperredundant robot resulted in high complexity in the calculation of the kinematic relationships necessary for control. With the help of D-H Parameter and pseudo inverses, a proposal for solving these problems was presented.

A demonstrator was developed to partially verify the conceptual considerations. This takes the ideas developed for the concept and reproduces the robotic structure on a smaller scale. Two segments coupled with Bowden cables were built as hardware. The first could perform a movement in the horizontal plane, whereas the second had two DOF in the vertical as well as in the horizontal plane. The system was completed with a linear axis for translation, an actuator box for decentralised control of the joints and a toolhead with grippers and camera. In addition, the necessary electronics were purchased, adapted to the demonstrator and set up. On the software side, a distributed system was developed that was controlled by a master controller. The master controller received user inputs via a gamepad and converted them into motion commands for the motion controllers within the nodes of a ROS-based programme. These took over the control of the drives and received their commands from the master controller via an EtherCAT field bus. In order to enable the user to visualise the images taken by the toolhead, an easy-to-use camera web server was set up. The demonstrator met the structural requirements as well as those set for mobility and operability, as verified in experiments.

Overall, the task set for the master's thesis can be described as fulfilled. With regard to vacuum compatibility, a housing and a pumping mechanism still need to be developed in the next steps. The software also needs to be further refined, as it currently only meets the still relatively simple requirements of the demonstrator. With the potentiometers mounted on the joints, an even more precise control algorithm in the form of a *dual-loop control* could possibly be realised. Furthermore, the developed CAD models could be used to build a simulation environment. With the help of the 3D scans of the interior of ASDEX Upgrade made by the

Max Planck Institute for Plasma Physics, path planning algorithms could be developed and methods for collision avoidance applied. Innovations can also be initiated with regard to instrumentation. Image recognition methods, for example, could be used to automatically detect damage.

Bibliography

[1] Akao, Y. *Quality function deployment : integrating customer requirements into product design*. Cambridge, Mass: Productivity Press, 1990. ISBN: 9781563273131.

[2] *Ansys Mechanical*. Accessed 2021-11-11. URL: https://www.ansys.com/products/structures/ansys-mechanical.

[3] *Arduino IDE*. Accessed: 2021-11-21. URL: https://www.arduino.cc/en/software.

[4] Asane, D., Schmitz, A., and Sugano, S. "Investigating the Strain Behaviour of Dyneema under Cyclic Loads". In: *The Proceedings of JSME annual Conference on Robotics and Mechatronics (Robomec)* 2020.0 (2020), 1P2–K05. DOI: 10.1299/jsmermd.2020.1p2-k05.

[5] Azizov, E. A. "Tokamaks: from A D Sakharov to the present (the 60-year history of tokamaks)". In: *Physics-Uspekhi* 55.2 (Feb. 2012), pp. 190–203. DOI: 10.3367/ufne.0182.201202j.0202.

[6] Becquet, M. "Some Key Issues in Remote Handling". In: *Teleoperation: Numerical Simulation and Experimental Validation*. Springer Netherlands, 1992, pp. 1–5. DOI: 10.1007/978-94-011-2648-9_1.

[7] Bourdelle, C., Artaud, J., Basiuk, V., Bécoulet, M., Brémond, S., Bucalossi, J., Bufferand, H., Ciraolo, G., Colas, L., Corre, Y., Courtois, X., Decker, J., Delpech, L., Devynck, P., Dif-Pradalier, G., Doerner, R., Douai, D., Dumont, R., Ekedahl, A., Fedorczak, N., Fenzi, C., Firdaouss, M., Garcia, J., Ghendrih, P., Gil, C., Giruzzi, G., Goniche, M., Grisolia, C., Grosman, A., Guilhem, D., Guirlet, R., Gunn, J., Hennequin, P., Hillairet, J., Hoang, T., Imbeaux, F., Ivanova-Stanik, I., Joffrin, E., Kallenbach, A., Linke, J., Loarer, T., Lotte, P., Maget, P., Marandet, Y., Mayoral, M., Meyer, O., Missirlian, M., Mollard, P., Monier-Garbet, P., Moreau, P., Nardon, E., Pégourié, B., Peysson, Y., Sabot, R., Saint-Laurent, F., Schneider, M., Travère, J., Tsitrone, E., Vartanian, S., Vermare, L., Yoshida, M., and and, R. Z. "WEST Physics Basis". In: *Nuclear Fusion* 55.6 (May 2015), p. 063017. DOI: 10.1088/0029-5515/55/6/063017. URL: https://doi.org/10.1088/0029-5515/55/6/063017.

[8] Bucalossi, J. "Tore Supra—WEST". In: *Magnetic Fusion Energy*. Elsevier, 2016, pp. 261–293. DOI: 10.1016/b978-0-08-100315-2.00009-x.

[9] Buckingham, R. and Graham, A. "Nuclear snake-arm robots". In: *Industrial Robot: An International Journal* 39.1 (Jan. 2012), pp. 6–11. DOI: 10.1108/01439911211192448.

[10] *CATIA V5R21 - Dessault Systems*. Accessed 2021-11-11. URL: https://www.3ds.com/.

[11] Craig, J. *Introduction to robotics : mechanics and control*. Upper Saddle River, N.J: Pearson/Prentice Hall, 2005. ISBN: 0131236296.

[12] Crooks, W., Vukasin, G., O'Sullivan, M., Messner, W., and Rogers, C. "Fin Ray® Effect Inspired Soft Robotic Gripper: From the RoboSoft Grand Challenge toward Optimization". In: *Frontiers in Robotics and AI* 3 (Nov. 2016). DOI: 10.3389/frobt.2016.00070.

[13] *Easy-Mechatronics System 1620A*. Accessed: 2021-11-21. URL: https://www.dold-mechatronik.de/Linearachse-Konfigurator-Easy-Mechatronics-System-1620A.

[14] Endo, G., Horigome, A., and Takata, A. "Super Dragon: A 10-m-Long-Coupled Tendon-Driven Articulated Manipulator". In: *IEEE Robotics and Automation Letters* 4.2 (Apr. 2019), pp. 934–941. DOI: 10.1109/lra.2019.2894855.

[15] *Espressif ESP32*. Accessed: 2021-11-21. URL: https://www.espressif.com/en/products/socs/esp32.

[16] *EtherCAT Technology Group*. Accessed: 2021-11-21. URL: https://www.ethercat.org/default.htm.

[17] *Faulhaber Homepage*. https://www.faulhaber.com/de/startseite/. Accessed: 2021-11-11.

[18] Fowler, K. R. "Introduction to Good Development". In: Elsevier, 2015, pp. 1–38. DOI: 10.1016/b978-0-12-405879-8.00001-5.

[19] Gargiulo, L., Bayetti, P., Bruno, V., Hatchressian, J.-C., Hernandez, C., Houry, M., Keller, D., Martins, J.-P., Measson, Y., Perrot, Y., and Samaille, F. "Operation of an ITER relevant inspection robot on Tore Supra tokamak". In: 84.2-6 (June 2009), pp. 220–223. DOI: 10.1016/j.fusengdes.2008.11.043.

[20] *Github - Espressif CameraWebServer Example*. Accessed: 2021-11-21. URL: https://github.com/espressif/arduino-esp32/tree/master/libraries/ESP32/examples/Camera/CameraWebServer.

[21] Haberfellner, R., Weck, O. de, Fricke, E., and Vössner, S. *Systems Engineering*. Zürich: Springer International Publishing, 2019. ISBN: 9783280040683. DOI: 10.1007/978-3-030-13431-0.

[22] Herrmann, A. "Special issue on ASDEX Upgrade". In: *Fusion Science and Technology* 44.3 (Nov. 2003). (guest editor). DOI: 10.13182/fst03-a399.

[23] Holtkamp, N. "An overview of the ITER project". In: *Fusion Engineering and Design* 82.5-14 (Oct. 2007), pp. 427–434. DOI: 10.1016/j.fusengdes.2007.03.029.

[24] Horigome, A. and Endo, G. "Basic study for drive mechanism with synthetic fiber rope – investigation of strength reduction by bending and terminal fixation method". In: *Advanced Robotics* 30.3 (Feb. 2016), pp. 206–217. DOI: 10.1080/01691864.2015.1102649.

[25] Houry, M., Gargiulo, L., Balorin, C., Bruno, V., Keller, D., Roche, H., Kammerer, N., Measson, Y., Carrel, F., and Schoepff, V. "Diagnostics carried by a light multipurpose deployer for vacuum vessel interventions". In: 86.9-11 (Oct. 2011), pp. 1868–1871. DOI: 10.1016/j.fusengdes.2010.11.004.

[26] *IGUS iglidur X*. Accessed: 2021-11-21. URL: https://www.igus.de/info/plain-bearings-x-material-data.

[27] *ISO 3529-1:2019-07 Vakuumtechnik; Verzeichnis von Fachausdrücken und Definitionen; Teil 1: Allgemeine Ausdrücke*. Norm. July 2019.

[28] Kiréanski, M. V. and Petrovié, T. M. "Combined Analytical- Pseudoinverse Inverse Kinematic Solution for Simple Redundant Manipulators and Singularity Avoidance". In: *The International Journal of Robotics Research* 12.2 (Apr. 1993), pp. 188–196. DOI: 10.1177/027836499301200207.

[29] Kolachalama, S. and Lakshmanan, S. "Continuum Robots for Manipulation Applications: A Survey". In: *Journal of Robotics* 2020 (July 2020), pp. 1–19. DOI: 10.1155/2020/4187048.

[30] Kutuvan, J. "Remote Handling Technology in Nuclear Industry". In: *Modern Manufacturing India* 1 (May 2013), pp. 22–25.

[31] Lee, J. K., Park, B. S., Lee, H. J., Kim, K., and Kim, H.-D. "Master-slave servo manipulator system for the PRIDE facility". In: *2010 1st International Conference on Applied Robotics for the Power Industry*. 2010, pp. 1–5. DOI: 10.1109/CARPI.2010.5624414.

[32] Liu, T., Mu, Z., Wang, H., Xu, W., and Li, Y. "A Cable-Driven Redundant Spatial Manipulator with Improved Stiffness and Load Capacity". In: *2018 IEEE/RSJ International Conference on Intelligent Robots and Systems (IROS)*. IEEE, Oct. 2018. DOI: 10.1109/iros.2018.8593679.

[33] Liu, T., Xu, W., Yang, T., and Li, Y. "A Hybrid Active and Passive Cable-Driven Segmented Redundant Manipulator: Design, Kinematics, and Planning". In: *IEEE/ASME Transactions on Mechatronics* 26.2 (Apr. 2021), pp. 930–942. DOI: 10.1109/tmech.2020.3013658.

[34] Liu, Y., Yan, Q., Zhang, Q., Guo, W., Odbal, Wu, B., and Wang, Z. "Control System Design and Implementation of Flexible Multi-joint Snake-Like Robot for Inspecting Vessel". In: Springer International Publishing, 2017, pp. 1037–1047. DOI: 10.1007/978-3-319-48036-7_76.

[35] Lou, Y., Quan, P., Lin, H., Wei, D., and Di, S. "A Closed-Form Solution for the Inverse Kinematics of the 2n-DOF Hyper-Redundant Manipulator Based on General Spherical Joint". In: *Applied Sciences* 11.3 (Jan. 2021), p. 1277. DOI: 10.3390/app11031277.

[36] *Maxon Aposs IDE*. Accessed: 2021-11-21. URL: https://www.maxongroup.ch/maxon/view/content/motion-controller.

[37] *Maxon Homepage*. https://www.maxongroup.de/maxon/view/content/index. Accessed: 2021-11-11.

[38] Motaleb, A. K. B., Hoque, M. B., and Hoque, M. A. "Bomb disposal robot". In: *2016 International Conference on Innovations in Science, Engineering and Technology (ICISET)*. IEEE, Oct. 2016. DOI: 10.1109/iciset.2016.7856510.

[39] Muhlich, P., Hamacher, T., Hartmann, T., Ward, D., Han, W., Tosato, G. C., Eherer, C., Biberacher, M., Silva, C. A. S., Pina, A., Gracceva, F., Ciorba, U., Grohnheit, P. E., Lechon, Y., and Cabal Cuesta, H. *The Potential Role for Fusion Power in Future Energy Markets*. Tech. rep. IAEA-CN–180. International Atomic Energy Agency (IAEA), 2010, p. 565. URL: http://inis.iaea.org/search/search.aspx?orig_q=RN:43046229.

[40] *OCRobotics*. visited on 2021-09-09. URL: https://www.ocrobotics.com.

[41] Oswald, Y., Owen, A., and Steinberger, J. K. "Large inequality in international and intranational energy footprints between income groups and across consumption categories". In: 5.3 (Mar. 2020), pp. 231–239. DOI: 10.1038/s41560-020-0579-8.

[42] Pan, H., Shi, S., Cheng, Y., and Zhao, W. "Progress and Prospects of EAST Remote Maintenance System". In: *2018 IEEE/RSJ International Conference on Intelligent Robots and Systems (IROS)*. IEEE, Oct. 2018. DOI: 10.1109/iros.2018.8594000.

[43] Peng, J., Xu, W., Yang, T., Hu, Z., and Liang, B. "Dynamic modeling and trajectory tracking control method of segmented linkage cable-driven hyper-redundant robot". In: *Nonlinear Dynamics* 101.1 (June 2020), pp. 233–253. DOI: 10.1007/s11071-020-05764-7.

[44] Perrot, Y., Cordier, J., Friconneau, J., Gargiulo, L., Martin, E., Palmer, J., and Tesini, A. "ITER articulated inspection arm (AIA): R&d progress on vacuum and temperature technology for remote handling". In: 75-79 (Nov. 2005), pp. 537–541. DOI: 10.1016/j.fusengdes.2005.06.028.

[45] Perrot, Y., Cordier, J., Friconneau, J., Maisonnier, D., Martin, E., and Palmer, J. "Development of a long reach articulated manipulator for ITER in vessel inspection under vacuum and temperature". In: 69.1-4 (Sept. 2003), pp. 187–190. DOI: 10.1016/s0920-3796(03)00334-x.

[46] *Raspberry Pi 4*. Accessed: 2021-11-21. URL: https://www.raspberrypi.com/products/raspberry-pi-4-model-b/.

[47] Rohde, V., Herrmann, A., Balden, M., Bösser, D., Hunger, K., Schall, G., Uhlmann, M., and Vierle, T. "Recovery from a hot water leakage at the tokamak ASDEX upgrade". In: 157 (Aug. 2020), p. 111630. DOI: 10.1016/j.fusengdes.2020.111630.

[48] *ROS - Robot Operating System*. Accessed: 2021-11-21. URL: https://www.ros.org.

[49] *Seeeduino XIAO*. Accessed: 2021-11-21. URL: https://wiki.seeedstudio.com/Seeeduino-XIAO/.

[50] Shi, S., Song, Y., Cheng, Y., Villedieu, E., Bruno, V., Feng, H., Wu, H., Wang, P., Hao, Z., Li, Y., Wang, K., and Pan, H. "Conceptual design main progress of EAST Articulated Maintenance Arm (EAMA) system". In: *Fusion Engineering and Design* 104 (Mar. 2016), pp. 40–45. DOI: 10.1016/j.fusengdes.2016.02.005.

[51] Tang, L., Wang, J., Zheng, Y., Gu, G., Zhu, L., and Zhu, X. "Design of a cable-driven hyper-redundant robot with experimental validation". In: *International Journal of Advanced Robotic Systems* 14.5 (Sept. 2017). DOI: 10.1177/1729881417734458.

[52] Tang, L., Zhu, L., Zhu, X., and Gu, G. "Confined spaces path following for cable-driven snake robots with prediction lookup and interpolation algorithms". In: *Science China Technological Sciences* 63.2 (Dec. 2019), pp. 255–264. DOI: 10.1007/s11431-019-1440-2.

[53] *Teufelberger Ocean 3000 XG*. Accessed 2021-11-21. URL: https://www.teufelberger.com/de/ocean-3000-xg.html.

[54] *Ultimaker S5*. Accessed: 2021-11-21. URL: https://ultimaker.com/de/3d-printers/ultimaker-s5.

[55] Villedieu, E., Bruno, V., Pastor, P., Gargiulo, L., Song, Y., Cheng, Y., Feng, H., Liu, C., and Shi, S. "An Articulated Inspection Arm for fusion purposes". In: 109-111 (Nov. 2016), pp. 1480–1486. DOI: 10.1016/j.fusengdes.2015.11.048.

[56] Walter, U. *Set of slides for the lecture in Systems Engineering, Technical University of Munich*. 2020.

[57] Wang, M., Dong, X., Ba, W., Mohammad, A., Axinte, D., and Norton, A. "Design, modelling and validation of a novel extra slender continuum robot for in-situ inspection and repair in aeroengine". In: *Robotics and Computer-Integrated Manufacturing* 67 (Feb. 2021), p. 102054. DOI: 10.1016/j.rcim.2020.102054.

[58] Wang, Y. *Space Robotics*. Springer Singapore, 2021. DOI: 10.1007/978-981-15-4902-1.

[59] Woolf, A. "Viking Kings of Britain and Ireland: The Dynasty of Ívarr to A.D. 1014 - By Clare Downham". In: *Early Medieval Europe* 16.4 (Oct. 2008), pp. 495–497. DOI: 10.1111/j.1468-0254.2008.240_2.x.

[60] Wu, B., Zeng, L., Zheng, Y., Zhang, S., Zhu, X., and Xu, K. "A Closed-Loop Controller for Cable-Driven Hyper-Redundant Manipulator with Joint Angle Sensors". In: *2019 IEEE International Conference on Robotics and Biomimetics (ROBIO)*. IEEE, Dec. 2019. DOI: 10.1109/robio49542.2019.8961405.

[61] Wu, B., Guo, W., Liu, Y., Zhang, Q., Zhou, L., Yan, Q., Zheng, Z., and Wang, Z. "Structural Design of Multi-joint Foldable Robot Manipulator for Remote Inspection in Experimental Advanced Superconducting Tokamak (EAST)". In: Springer International Publishing, 2017, pp. 993–1002. DOI: 10.1007/978-3-319-48036-7_72.

[62] Wu, S. "An overview of the EAST project". In: *Fusion Engineering and Design* 82.5-14 (Oct. 2007), pp. 463–471. DOI: 10.1016/j.fusengdes.2007.03.012.

[63] Wu, Z., Wu, B., and Wang, Z. "Kinematic and Dynamic Analysis of a In-Vessel Inspection Robot System for EAST". In: 34.5 (May 2015), pp. 1203–1209. DOI: 10.1007/s10894-015-9939-y.

[64] Wu, Z., Wu, B., Zhang, Q., and Wang, Z. "Development and Analysis of a Long Reach Robot for EAST Vacuum Vessel Inspection". In: 34.5 (Mar. 2015), pp. 983–988. DOI: 10.1007/s10894-015-9907-6.

[65] Wutz, M., Adam, H., Walcher, W., and Jousten, K. *Handbuch Vakuumtechnik*. Vieweg Teubner Verlag, 2000. DOI: 10.1007/978-3-322-99947-4.

[66] Xu, W., Mu, Z., Liu, T., and Liang, B. "A modified modal method for solving the mission-oriented inverse kinematics of hyper-redundant space manipulators for on-orbit servicing". In: *Acta Astronautica* 139 (Oct. 2017), pp. 54–66. DOI: 10.1016/j.actaastro.2017.06.015.

[67] Yates, J. T. "Motion in Vacuum". In: Springer International Publishing, 2015, pp. 3–38. DOI: 10.1007/978-3-319-17668-0_1.

[68] Yeshmukhametov, A., Buribayev, Z., Amirgaliyev, Y., Amirgaliyev, B., and Latuta, K. "Bio-inspired a novel continuum robot arm with variable backbone design: modelling and validation". In: *Journal of Theoretical and Applied Information Technology* 97 (Oct. 2019), p. 19.

[69] Zammuto, I., Giannone, L., Herrmann, A., Houben, A., Kallenbach, A., Schuhbeck, K., Sieglin, B., and Vorbrugg, S. "Implementation of ferritic steel as in vessel wall: Lessons learnt and follow up". In: 124 (Nov. 2017), pp. 297–301. DOI: 10.1016/j.fusengdes.2017.04.016.

Disclaimer

I hereby declare that this thesis is entirely the result of my own work except where otherwise indicated. I have only used the resources given in the list of references.

Garching, December 7, 2021

(Signature)